МІНІСТЕРСТВО ОСВІТИ І НАУКИ УКРАЇНИ

НАЦІОНАЛЬНИЙ АВІАЦІЙНИЙ УНІВЕРСИТЕТ

КАФЕДРА КОНСТРУКЦІЇ ЛІТАЛЬНИХ АПАРАТІВ

ДОПУСТИТИ ДО ЗАХИСТУ
Завідувач кафедри
д.т.н., професор
_____Сергій ІГНАТОВИЧ
«___ »_____2022 р.

КВАЛІФІКАЦІЙНА РОБОТА
ВИПУСКНИКА ОСВІТНЬОГО СТУПЕНЯ МАГІСТРА
ЗІ СПЕЦІАЛЬНОСТІ
«АВІАЦІЙНА ТА РАКЕТНО-КОСМІЧНА ТЕХНІКА»

Тема: «Конструктивне проектування лонжеронів крила з композиційних матеріалів»

Виконавець: _____ **ВАН Цінле**

Керівник: к.т.н., доцент _____ **Тетяна МАСЛАК**

Охорона праці: к.т.н., доцент _____ **Катерина КАЖАН**

Охорона навколишнього середовища:

к.т.н., професор _____ **Леся ПАВЛЮХ**

Нормоконтролер: к.т.н., доцент _____ **Володимир КРАСНОПОЛЬСЬКИЙ**

Київ 2022

MINISTRY OF EDUCATION AND SCIENCE OF UKRAINE

NATIONAL AVIATION UNIVERSITY

DEPARTMENT OF AIRCRAFT DESIGN

PERMISSION TO DEFEND
Head of the department,
Dr. of Sc., professor
_____ Sergiy IGNATOVYCH
"___" _____ 2022

MASTER DEGREE THESIS
ON SPECIALITY
"AVIATION AND ROCKET-SPACE TECHNOLOGIES"

Topic: "Structural design of composite wing spars"

Fulfilled by:	**_____**	**WANG Qingle**
Supervisor: **PhD, associate professor**	**_____**	**Tetiana MASLAK**
Labor protection advisor: **PhD, associate professor**	**_____**	**Katerina KAZHAN**
Environmental protection adviser: **PhD, professor**	**_____**	**Lesya PAVLYUKH**
Standards inspector: **PhD, associate professor**	**_____**	**Volodymyr KRASNOPOLSKYI**

Kyiv 2022

НАЦІОНАЛЬНИЙ АВІАЦІЙНИЙ УНІВЕРСИТЕТ

Факультет аерокосмічний

Кафедра конструкції літальних апаратів

Освітній ступінь «Магістр»

Спеціальність 134 «Авіаційна та ракетно-космічна техніка»

Освітньо-професійна програма «Обладнання повітряних суден»

ЗАТВЕРДЖУЮ
Завідувач кафедри
д.т.н., професор
_____Сергій ІГНАТОВИЧ
«___» _____2022 р.

ЗАВДАННЯ

на виконання кваліфікаційної роботи пошукача

ВАН Цінле

1. Тема роботи **«**Конструктивне проектування лонжеронів крила з композиційних матеріалів**»**, затверджена наказом ректора від 05 жовтня 2022 року №1861/ст.
2. Термін виконання роботи: з 06 жовтня 2022 р. по 30 листопада 2022 р.
3. Вихідні дані до роботи: геометричні параметри крила, механічні характеристики конструкційних матеріалів.
4. Зміст пояснювальної записки: застосування композиційних матеріалів в авіації, принципи моделювання композиційних конструкцій, моделювання конструкції лонжерона крила для широкофюзеляжного далекомагістрального літака, вибір форми поперечного перерізу лонжерона крила та визначення його пружно-деформованого стану, питання охорони праці та навколишнього середовища.
5. Перелік обов’язкового графічного (ілюстративного) матеріалу: презентація Power Point, малюнки та схеми.

6. Календарний план-графік:

№	Завдання	Термін виконання	Відмітка про виконання
1	Огляд літератури про застосування композиційних матеріалів, їх технологію виготовлення та принципи моделювання	06.10.2022-18.10.2022	
2	Аналіз принципів моделювання композиційних конструкцій	19.10.2022-29.10.2022	
3	Вибір форми конструкції лонжеронів крила, вибір конструкційного матеріалу	30.10.2022-07.11.2022	
4	Моделювання лонжерона та визначення його пружно-деформованого стану	06.10.2022-31.10.2022	
5	Виконання розділів, присвячених охороні навколишнього середовища та праці	01.11.2022-04.11.2022	
6	Оформлення кваліфікаційної роботи	05.11.2022-10.11.2022	

7. Консультанти з окремих розділів:

Розділ	Консультанти	Дата, підпис	
		Завдання видав	Завдання прийняв
Охорона праці	к.т.н., доцент Катерина КАЖАН		
Охорона навколишнього середовища	к.т.н., професор Леся ПАВЛЮХ		

8. Дата видачі завдання: 5 жовтня 2022 р.

Керівник кваліфікаційної роботи: _____ Тетяна МАСЛАК

Завдання прийняв до виконання: _____ ВАН Цінле

NATIONAL AVIATION UNIVERSITY

Aerospace Faculty

Department of Aircraft Design

Educational Degree "Master"

Specialty 134 "Aviation and Rocket-Space Technologies"

Educational Professional Program "Aircraft Equipment"

APPROVED BY

Head of Department,

Dr. of Sc., professor

_____ Sergiy IGNATOVYCH

"___" _____ 2022

TASK

for the master degree thesis

WANG Qingle

1. Topic: "Structural Design of Composite Wing Spars", approved by the Rector's order № 1861/ст from 05 October 2022 year.
2. Period of work execution: from 05 October 2022 year to 30 November 2022 year.
3. Initial data: wing geometry, mechanical properties of structural materials.
4. Content: application of composite materials in aviation, modeling principles of composite structures, finite element modeling of the wing spar for the wide-body long range aircraft, the stress-strain analysis of the wing spar, labor and environmental protection.
5. Required material: Power Point Presentation, drawings and diagrams.

6.Thesis schedule:

№	Task	Time limits	Done
1	Literature overview of composite materials implementation, manufacturing technology	06.10.2022-18.10.2022	
2	Analysis of principles of composite structures modeling	19.10.2022-29.10.2022	
3	The choice of wing spar cross-section and choice of the structural materials	30.10.2022-07.11.2022	
4	Spar modeling and stress-strain analysis of it	06.10.2022-31.10.2022	
5	Implementation of the parts, devoted to environmental and labor protection	01.11.2022-04.11.2022	
6	Edit and correct the draft, modify the format	05.11.2022-10.11.2022	

7. Special chapter advisers:

Chapter	Adviser	Date, signature	
		Task issued	Task received
Labor protection	PhD, associate professor Katerina KAZHAN		
Environmental protection	PhD, professor Lesya PAVLYUKH		

8. Date of issue of the task: 8 September 2022 year.

Supervisor: _____ Tetiana MASLAK

Student: _____ WANG Qingle

РЕФЕРАТ

Пояснювальна записка до кваліфікаційної роботи на тему "Конструктивне проектування лонжеронів крила з композиційних матеріалів"

82 сторінки, 38 рисунків, 12 таблиць, 32 джерел

В представленій кваліфікаційній роботі об’єктом дослідження є аналіз пружно-деформованого стану конструктивного елемента крила. Предметом дослідження є вибір форми поперечного перерізу лонжерона крила, визначення його міцнісних характеристик при рівнях навантажень, що виникають в конструктивному елементі широкофюзеляжного далекомагістрального літака.

Метою кваліфікаційної роботи є виконання аналізу пружно-деформованого стану лонжерона крила, виготовленого з композитного матеріалу.

Методами дослідження є: аналіз наукових робіт з впровадження композиційних матеріалів в авіації, аналіз принципів їх моделювання, аналіз навантаження основних елементів несучої конструкції крила, моделювання форми поперечного перерізу лонжерона крила, аналіз прежно-деформованого стану та вибір матеріалів.

Кваліфікаційна робота включає аналіз використання композитних матеріалів для основних несучих елементів крила. Композитні матеріали мають ряд переваг у порівнянні з алюмінієвими сплавами, тому широко використовуються в аерокосмічній галузі [1]. Відповідно до вимог до основних елементів крила – високої жорсткості, високої міцності та малої ваги, використання тонкостійної композитної конструкції лонжеронів крила дає можливість реалізувати конструктивну цілісність та легкість балки великої довжини.

Практична цінність роботи полягає у виконанні пружно-деформованого аналізу конструкції лонжерона крила з композиційного матеріалу. Матеріали кваліфікаційної роботи можуть бути використані в авіаційній промисловості та в навчальному процесі, пов'язаному з вивченням конструкції та міцності літака.

Літак, крило, лонжерон, композитні матеріали, метод скінченних елементів, пружно-деформований стан

ABSTRACT

Master degree thesis "Structural design of composite wing spars"

82 pages, 38 figures, 12 tables, 32 references

Object of study is the stress-strain analysis of the structural elements of the wing.

Subject of study is the analysis of different shape of the wing spar and its bearing performances under loading for the wide-body long range passenger aircraft.

Aim of master degree thesis is to perform the stress-strain analysis of the wing spar made of composite material.

Research and development methods are analysis the existing research works on the implementation of composite materials in aviation, the analysis of principles of their modeling, analysis of loading of the main bearing structure elements of the wing, modeling of the shape of wing spar cross section with the stress-strain analysis and with the choice of materials which suit the best.

The thesis consists of analysis of the usage of composite materials for the main bearing elements of the wing. Composite materials have a number of advantages compared to aluminum alloys, so they are widely used in the aerospace industry [1]. According to the requirements of high stiffness, high strength and light weight of the main beam of the aircraft wing, the thin-layer composite material is easy to realize the structural lightweight of the long-span main beam.

Practical value of the work is proved by the performing of stress-strain analysis of the wing spar structure made of composite material.

The materials of the master's thesis can be used in the aviation industry and in the educational process related to the learning of the aircraft design and strength.

Aircraft, wing, spar, composite materials, finite element analysis, stress-strain state

CONTENT

INTRODUCTION

Glass fibers first appeared in the United States in 1932. At the Wright-Patterson Air Force Base in 1943, exploratory projects were launched to build structural aircraft parts from composite materials. This resulted in the first plane with a GFRP fuselage being flown on the base a year later [2]. After this, with the continuous emergence of new materials, new technologies and new processes, rubber-based composite materials have gradually developed into a class of materials with relatively mature technology and a wide range of applications. The application on aerospace vehicles has gradually developed from accessory parts and secondary load-bearing parts to main load-bearing parts.

When design the aircraft structure, reducing the structural weight is very prominent. How to achieve the requirements of light weight, large span, high structural rigidity and strength has become the focus and difficulty in the design of aircraft wings, especially with the main spar of the wing.

There are generally three ways to achieve the improvement of structural bearing capacity and light weight: material, structure and manufacturing process. The weight of load-bearing structural members can be effectively reduced by selecting lighter and higher-strength materials, adopting a structural configuration with higher bearing efficiency, and improving the manufacturing process. Especially developing the overall manufacturing technology to reduce the redundant connection of each structural member. Thin layer composites, which have become a research hotspot in recent years, have better mechanical properties than standard and thick-ply composites. After reducing the ply thickness, the laminated composite material has higher ply design "space" and "freedom", and also obtains higher material mechanical strength properties. The application of thin-layer composite materials to the design of wing main beams can further improve the bearing efficiency of the main beams, reducing structural weight and improve structural safety.

Although composite has been initially used in some aerospace vehicles, they are still in the exploratory stage as long-span main bearing structures; in addition, the research on the mechanical behavior of thin-layer composites is not mature, and the application of thin-layer composites is still in the exploratory stage. It is still in the preliminary research stage

of the composite material structure. Therefore, it has high academic value and engineering application to carry out experimental and theoretical analysis of the mechanical properties of thin-layer composite materials, to deeply understand the mechanism of their mechanical properties improvement and promote their application in composite structural parts. The design, analysis and testing of the thin-layer composite structure wing beam is of great significance to promote the application of composite structure as the main bearing structure in aerospace vehicles.

The main goals of the presented qualification work are:

- to perform the analysis of the wing spar structures of the wide body aircraft to find the best cross-sections of the wing spars which are commonly used;
- to simulate the compression tests for all types of the wing spar
- to perform the stress-strain analysis of the presented types of the wing spars
- to analyze the materials for the structural element.

PART 1. COMPOSITE MATERIALS IN AVIATION APPLICATION

1.1 Development of composite structures

In view of the superiority of composite materials in aircraft structure, Europe and the United States attach great importance to the research of composite aircraft structure technology. The application of composite materials in civil aircraft can be roughly divided into four stages.

In the first stage, starting in the early 1970s, composite materials were mainly used in components with less stress, such as flaps, spoilers, leading edges and fairings.

In the second stage, in the mid-1980s, rudders, elevators, flaps, ailerons and other relatively low load-bearing components began to be manufactured by composite materials.

In the third stage, composite materials have been introduced to larger load-bearing structures such as vertical tails and tails. Among them, the Boeing 777 with composite horizontal tail and vertical tail uses a total of 9.9 tons of composite materials, accounting for 11% of the total weight of the structure. Figure 1.1 shows the application of composite materials in some civil aircraft.

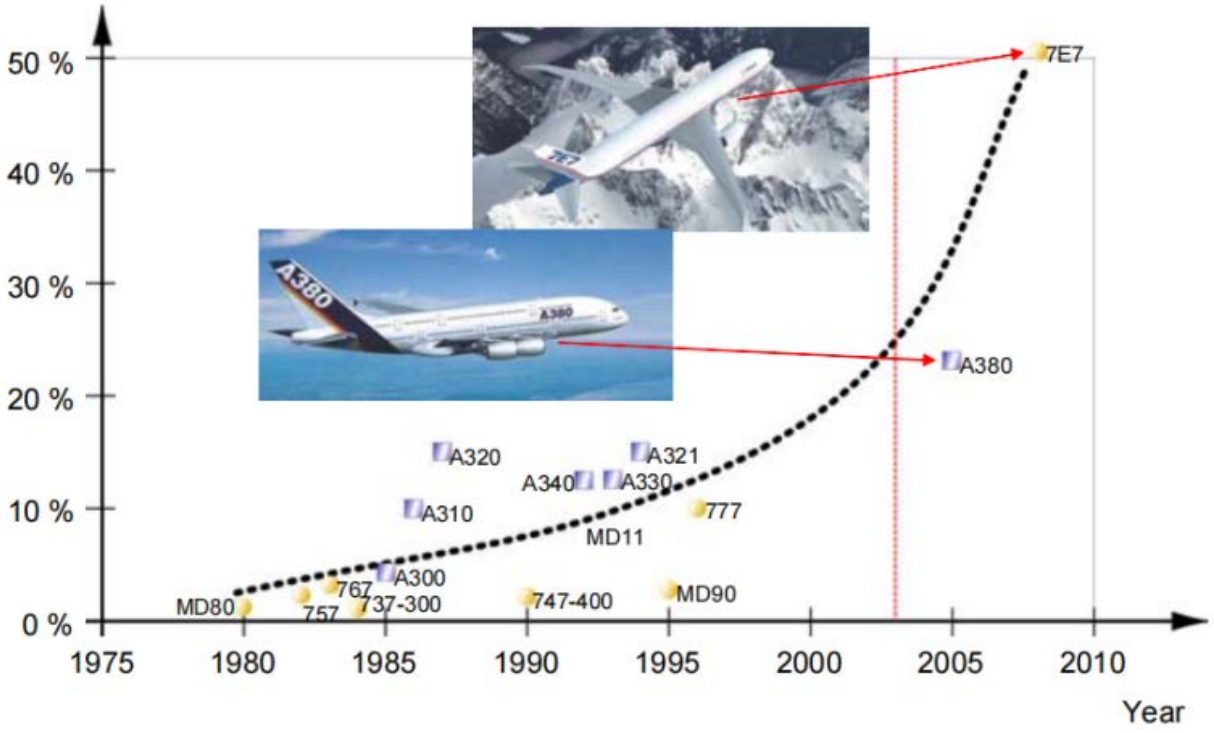

Figure 1.1 – the development of composite aerospace applications

In the fourth stage, the wing and fuselage have also adopted composite materials as the main stress-bearing components. Such as Boeing 787, see Figure 1.2. The composite material consumption of Boeing 787 is 50% [3], which has exceeded the sum of aluminum, steel, titanium and other metal materials. Among them, composite materials are mainly used in the fuselage, wings, horizontal tail, vertical tail and other parts. Boeing 787 leads the development trend of composite aircraft.

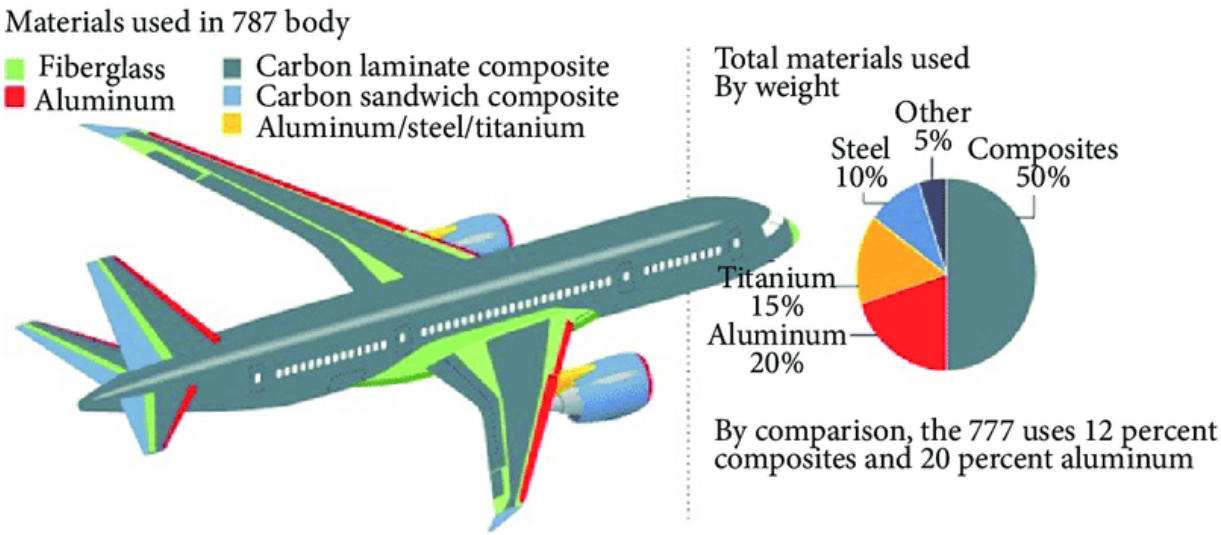

Figure 1.2 – Usage of various materials in the Boeing 787 Dreamliner

The use of carbon-fiber components in the aviation industry is becoming more and more common. But for Airbus, Carbon Fiber Reinforced Plastic (CFRP) components are nothing new.

Airbus has used carbon-fiber materials for many years. Starting with the A310-200 in 1983 when the spoilers, air brakes and rudder were made of sandwich CFRP. Three years later, the A310-300 pioneered the introduction of composite on a primary structure with the vertical tail plane designed in monolithic CFRP. On the A320, carbon-fiber materials were used on flaps, ailerons, spoilers and on the vertical and horizontal tail planes. On the A340-600 the rear pressure bulkhead and keel beams were made of CFRP. On the A380, Airbus introduced them in the fuselage rear section and center wing box connecting the two wings together, while the wing ribs moved to carbon-fiber. This evolution continued on the A350 XWB where the entire fuselage and wing skins – more than half of the structure - is made

from carbon-fiber composites [4]. As shown in figure 1.3, the Airbus A350 XWB uses up to 53% composite materials and 14% titanium alloys.

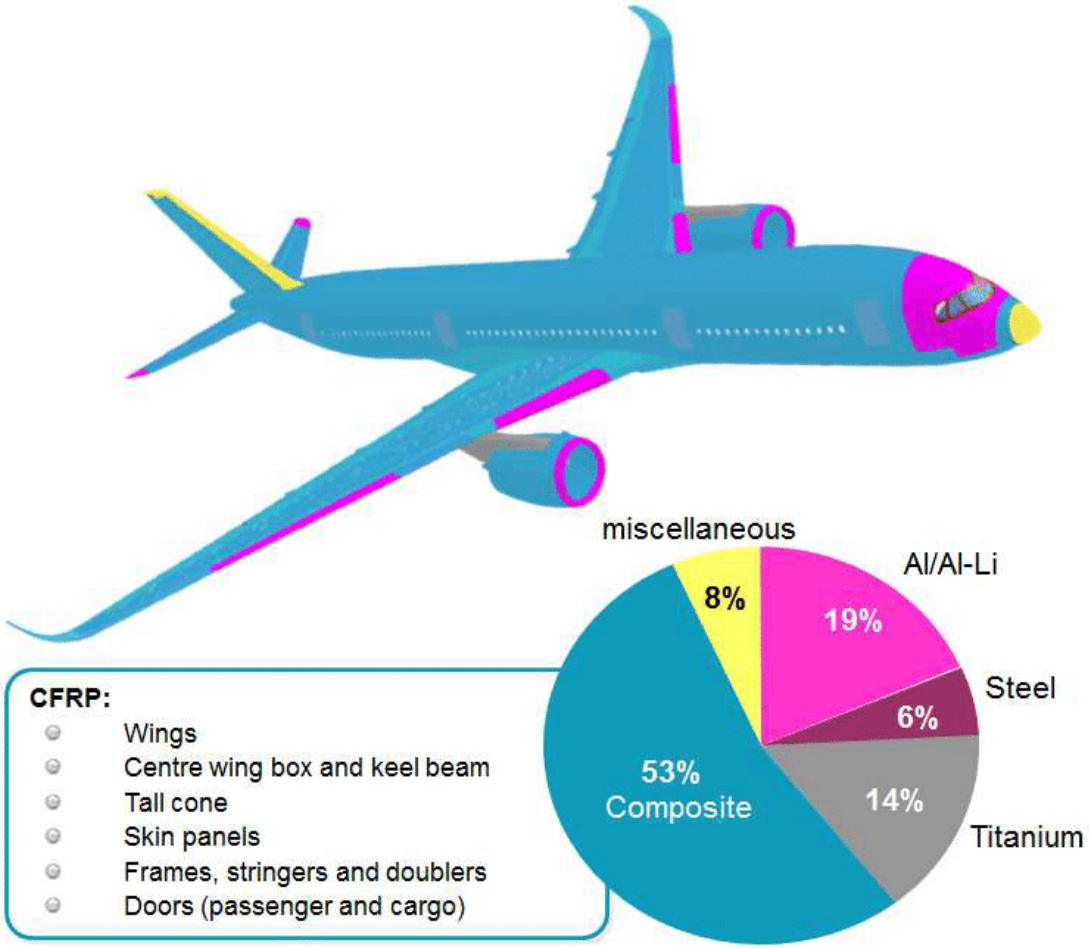

Figure 1.3 – Usage of various materials in the A350 XWB

High specific strength, high specific stiffness, high degree of integration, and many other excellent characteristics make advanced composite materials widely use in aerospace structures. Its application in aircraft structure is 25~30% lighter than conventional metal materials, and can significantly improve aircraft aerodynamic characteristics. In addition, the advantages of composite materials such as easy integral molding, excellent fatigue resistance, and corrosion resistance greatly reduce the life-cycle cost of the structure. Nowadays, the application amount and application parts of advanced composite materials have become important indicators to measure structural advancement of aircraft. The main beam as the main bearing structure of the wing, the importance is self-evident.

Wing spar is the main load-bearing structure of civil aircraft, and due to the complex shape of the airfoil, there are many difficulties in design. As the main component of the

aircraft to generate lift, the wing is also increasingly using composite materials. The wing structure using composite materials not only meets the aerodynamic requirements of the wing, but also its strength and stiffness can better meet the stability and life requirements of the aircraft. At present, many scholars have carried out a series of theoretical research on the composite wing structure, which involves structural design, static analysis, dynamic analysis and structural optimization design.

Initially, although the specific strength of composite is much better than metal materials, but its specific stiffness is not high, and its structural weight reduction effect and structural mechanical properties are not ideal, so it has not been widely used in aircraft main load-bearing structures. With the advent of high-performance fibers such as carbon fiber and boron fiber in the 1960s, it became possible to widely use composite materials in aircraft structures. People also call high-performance fiber composite materials such as carbon fiber and boron fiber after glass fiber as advanced composite materials. At present, the most widely used composite materials is carbon fiber composite material, table 1.1 shows the mechanical properties of carbon fiber produced by Toray Company, Japan. From the initial low modulus and low strength T300 carbon fiber has developed to high strength T700~1000 series and high Modulus of the MJ and M-JB series.

Since the 1990s, the design of the components also focuses on the development of the manufacturing process while pursuing the performance. For this reason, the automatic wire laying and tape laying machine is developed to improve the production efficiency, product quality. In addition, an integrated structure design and fabrication technique based on co-curing/co-bonding has also been developed to greatly reduce the number of parts and costs.

Typical representatives of composite materials used in large aircraft are Airbus A380 and Boeing B787. The A380 successfully produced the composite central wing box. Only this is 1.5t lighter than the most advanced aluminum alloy material. Air brake, vertical and horizontal stabilizers, elevators, rudders, flap spoilers, ailerons, landing gear doors, vertical stabilizer boxes, fairings and so on are all made of carbon fiber composite materials.

Table 1.1

Mechanical properties of carbon fiber fabricated by Toray

Carbon Type		Tow	Tensile strength /MPa	Modulus /GPa	Density (g/cm^3)	Elongation /%
T300	T300-1000	1000	3530	230	1.76	1.5
	T300-3000	3000	3530	230	1.76	1.5
	T300-6000	6000	3530	230	1.76	1.5
	T300-12000	12000	3530	230	1.76	1.5
T400HB	T400HB-3000	3000	4410	250	1.80	1.8
T700SC	T700SC-12000	12000	4900	230	1.80	2.1
	T700SC-24000	24000	4900	230	1.80	2.1
T800SC	T800SC-24000	24000	5880	294	1.80	2.0
T800HB	T800HB-12000	12000	5490	294	1.81	1.9
T830HB	T830HB-6000	6000	5340	294	1.81	1.8
T1000GB	T1000GB-12000	12000	6370	294	1.80	2.2
T1000GC	T1000GC-12000	12000	7000	324	1.79	2.0
	T1000GC-24000	24000	7000	324	1.79	2.0
M35JB	M35JB-6000	6000	4510	343	1.75	1.3
	M35JB-12000	12000	4700	343	1.75	1.4
M40JB	M40JB-6000	6000	4400	377	1.77	1.2
	M40JB-12000	12000	4400	377	1.77	1.2
M46JB	M46JB-6000	6000	4200	436	1.84	1.0
	M46JB-12000	12000	4020	436	1.84	0.9
M50JB	M50JB-6000	6000	4120	475	1.88	0.9
M50J	M50J-6000	6000	4020	540	1.91	0.8
M55JB	M55JB-6000	6000	4020	540	1.91	0.8
M60JB	M60JB-3000	3000	3820	588	1.93	0.7
	M60JB-6000	6000	3820	588	1.93	0.7
M30SC	M30SC-18000	18000	5490	294	1.93	1.9

It is not difficult to see that the development trend of the composite materials in aircraft structures is that the amount of application is increasing and the scope of application is becoming more and more extensive.

1.2. Technology of layered composites

Thin-layer composite material refers to the composite material with relatively thin thickness of single layer, which is prepared by widening and thinning fiber bundles through certain stretching process. The thickness of the single layer (as shown in the figure 1.4) for preparing composite materials is usually 0.125~0.250 mm.

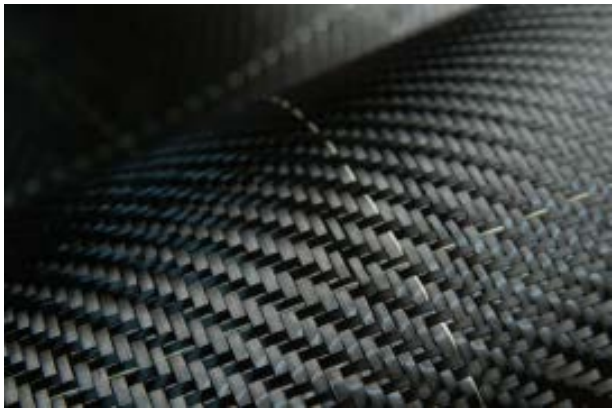

Figure 1.4 – Single layer of composite

When designing some composite structures, especially thin-walled structures, the limitation of the number of layers makes the design work harder, and the layer design is difficult to meet the requirements when subjected to multi-directional comprehensive load conditions. However, the advent of thin layup process technology has largely solved this problem. At present, the thickness of the prepreg prepared by the fiber tow extension process can be as thin as 0.015 mm, which is equivalent to about 1/8~1/16 of the conventional layup thickness (0.125~0.250 mm), the original single layer method (only one fiber orientation angle) now can choose various layer methods, such as symmetrical, orthogonal, balanced or quasi-isotropic, so as to "design space" and "design freedom" is greatly improved.

Considering a laminate manufactured using unidirectional (UD) plies, the layup notation is described as shown in the figure 1.5 [5]:

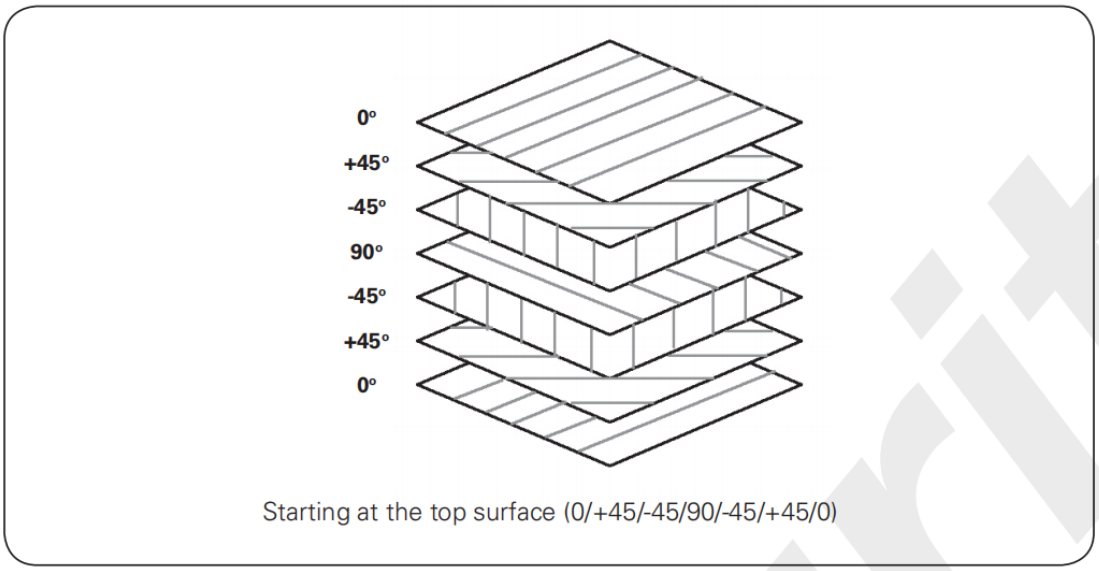

Figure 1.5 – Stacking sequence example

When designing a laminate, it is important to consider the stacking sequence of plies and to be aware of SYMMETRY and BALANCE of the stack. The stack above is both symmetric (about the mid plane) which helps to eliminate any tendency to bend or warp, and balanced meaning that there is an equal number of +45° & -45° plies, which reduces shear coupling.

The key to preparing thin-layer prepreg is the tow stretching process. At present, the tow stretching process generally adopts the rolling method, the negative pressure air flow method and the ultrasonic dispersion method.

The rolling method is to spread the prepreg of ordinary thickness on the preheating platform, heat the resin to maintain a certain fluidity, and use the flattening roller to exert pressure on it, supplemented by the action of the scraper, so that the fiber tow is under the action of pressure. It expands laterally with the flow of the resin, so as to achieve the effect of reducing the thickness. This method has low cost, but when the fiber is stretched, if the pressure of the flattening roller is too high, the internal fibers will be broken, and the mechanical properties of the finally produced laminate will be poor and cannot achieve fiber expansion effect.

As presented in [6], we can observe the process for stretching fiber bundles using negative pressure airflow, which can make 6 mm width carbon fiber tow stretch to 20 mm, and is approximately 1/3 thickness of the commonly used standard layup (0.125 mm). Figure

1.6 and figure 1.7 [7] show the principle of negative pressure airflow stretching the tow. An air pump is used in the chamber between the two fiber bundle guide rollers to form a negative pressure airflow environment. The air flow rate is different in different areas around the bundle, and the transverse aerodynamic force generated causes the fibers to be dispersed against the tension, so that the tow is spread out laterally. As shown in Figure 1.8, when the fiber passes through the guide rollers in the stretcher, the air pipes arranged in the chamber between the guide rollers suck the air above the fibers downward under the action of the vacuum pump, thereby forming orientation of negative pressure airflow. The tow is expanded under the action of the continuous stable airflow and the lateral aerodynamic effect, and due to the low airflow rate, the expansion process does less damage to the fiber.

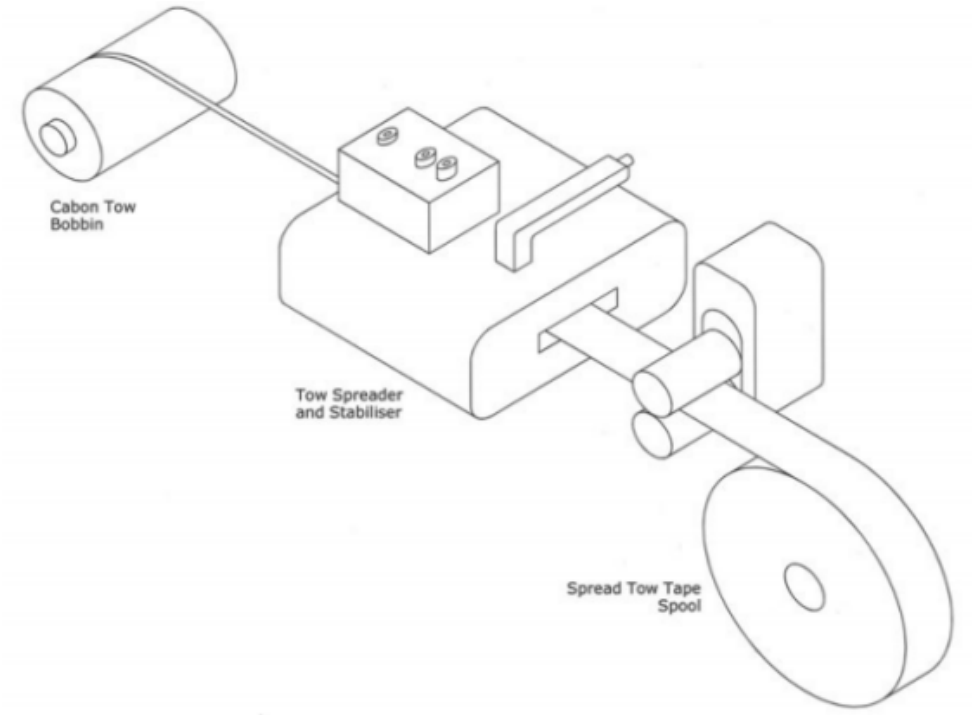

Figure 1.6 – Spreading fiber tows into thin tapes by Oxeon 2014

As presented in [8], we can observe that they used numerical simulations and experiments to study the effects of airflow distribution, boundary conditions, airflow rate, tow extending rate and number of fiber tows on the extending effect in the extending system. The system efficiently and uniformly thins 12 k carbon fiber tow up to 83% wide.

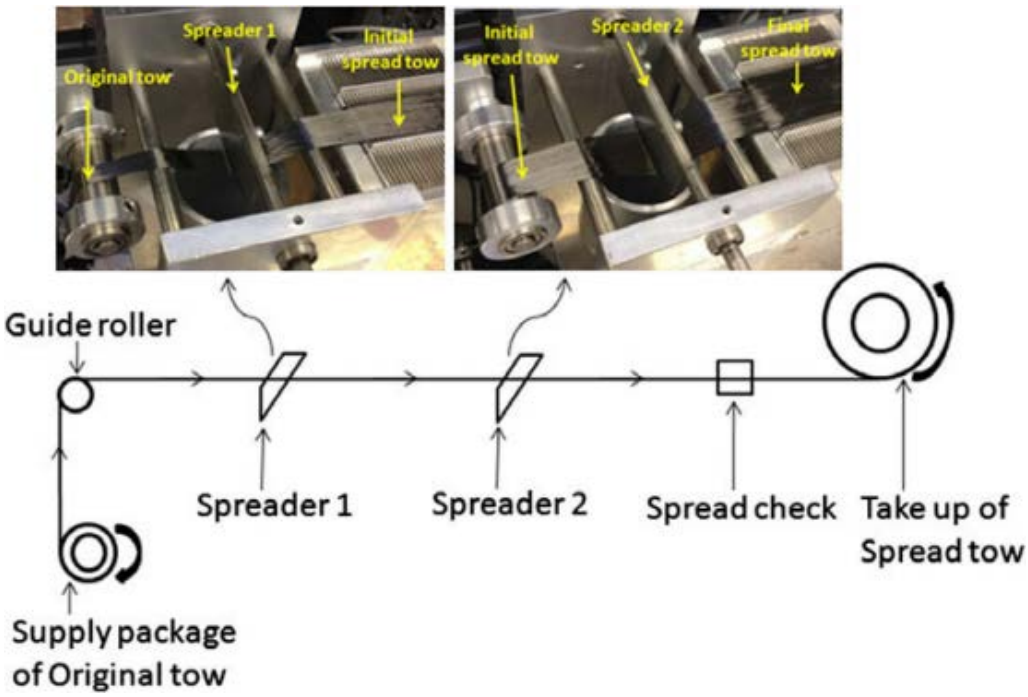

Figure 1.7 – Schematic of the air-flow tow-spreading technology (El-Dessouky, 2013)

The ultrasonic dispersion method is a fiber expansion method recently applied to the tow extension process. This method has the advantages of low fiber damage, improved fiber micro-curvature, and good stretching effect, which may become the mainstream tow stretching method in the future.

1.3. Mechanical properties of composite materials

Thin-ply fiber laminates exhibit higher in situ transverse strength or resistance against matrix cracking. The mechanical behaviors of standard-thickness-ply and thin-ply laminates have been compared, but only one kind of thin-ply thickness was considered [9-13]. This qualitative analysis just identified the superior mechanical properties of thin laminates compared to traditional laminates. But the optimal ply thickness cannot be obtained directly.

Recently, the mechanical properties of variable-ply laminates have been investigated. Thin plies in unidirectional or QSI (quasi-isotropic) laminates have been shown to increase monotonously strength or fracture toughness with the decrease of ply thickness [5]. On the contrary, some experimental results showed that with the decrease of ply thickness, the

strength or fracture toughness increase firstly and then decrease for cross-ply laminates or angle-ply laminates [5-7].

As presented in [14], we can observe that three different stacking sequences were designed using unidirectional ultra-thin ply prepreg (20 gsm). The stacking sequences of the cross-ply laminates of [0°/90°]12s, [0°3/90°3]4s and [0°6/90°6]2s, corresponded to fiber areal weights of 20, 60 and 120 g/m2, respectively. All the configurations had the same nominal thickness with a total of 48 plies and were symmetric around the mid-plane of the laminate.

Delamination is the typical damage mode under short-beam shear loading. Three mesh sizes along the X and Y directions (0.6, 0.3 and 0.15 mm) were considered. The displacement-load curves and the damage modes for the short-beam shear test are shown in Fig.1.8. Very similar linear stages and maximum loads are obtained using the three mesh sizes. The part of the degradation curve within the dotted circle corresponds to delamination propagation. Delamination was identified by element sliding. The degradation trends are similar for the 0.3- and 0.15-mm meshes. Although there are some differences between the degradation stage in the curve obtained using the 0.6-mm mesh and those obtained using the 0.3- and 0.15-mm meshes, delamination is the damage mode for all the mesh sizes. In general, the 0.3-mm mesh is sufficiently small to ensure accuracy for determining the maximum load or the damage modes.

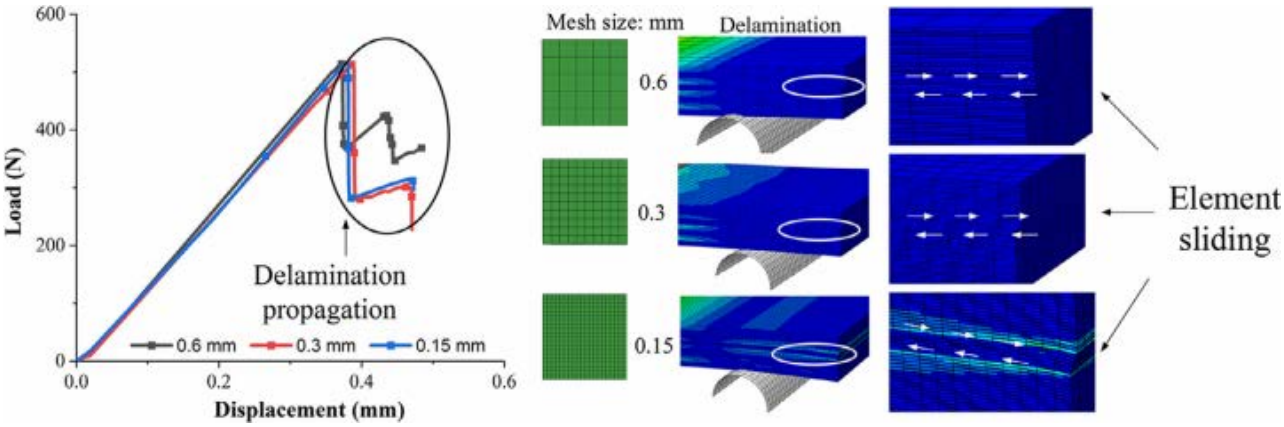

Figure 1.8 – Mesh size dependence of laminates under SBS test

As presented in [15], we could observe that CFRP unidirectional prepreg system produced by NTPT (North Thin Ply Technology, Switzerland), which is composed of NTPT's epoxy resin TP402 and T700S carbon fibers from Toray Carbon Fibers America, Inc. The target for the fiber volume content of the prepregs was 55%. The produced fiber area weights are 30 gsm, 60 gsm and 120 gsm. Higher fiber area weights such as 240 gsm and 360 gsm were produced by block-scaling an according to the number of same-oriented layers. The prepregs were cut by CNC cutter (Aristomat TL1625 from ARISTO Graphic System GmbH & Co. KG i.I., Germany) and manufactured by hand lay-up. The layers were debulked by a vacuum bag every fourth layer. Table 1.2 shows the used lay-ups.

Table 1.2

Laminate lay-ups

Test method	Fiber area weight in gsm				
	30	60	120	240(2X120)	360(3X120)
Tension	$[45/90/-45/0]_{12s}$	$[45/90/-45/0]_{6s}$	$[45/90/-45/0]_{3s}$	$[45_2/-45_2/90_2/0_2]_s$	$[45_3/-45_3/90_3/0_3]_s$
compression	$[45/90/-45/0]_{22s}$	$[45/90/-45/0]_{11s}$	$[45/90/-45/0]_{6s}$	$[45_2/90_2/-45_2/0_2]_{3s}$	$[45_3/-45_3/90_3/0_3]_{2s}$
Fatigue	$[45/90/-45/0]_{12s}$	$[45/90/-45/0]_{6s}$	$[45/90/-45/0]_{3s}$	_	$[45_3/-45_3/90_3/0_3]_s$
FAI	$[45/90/-45/0]_{12s}$	$[45/90/-45/0]_{6s}$	$[45/90/-45/0]_{3s}$	_	$[45_3/-45_3/90_3/0_3]_s$

The results of the tension-tension tests are shown in Fig.1.9. At least five samples were tested for each configuration. Table 1.3 shows the number of tested samples for each ply thickness and load case.

The tensile strength increases significantly with decreasing layer thickness in the range between 360 gsm and 60 gsm. Even lower layer thicknesses, 30 gsm, show no further improvement compared to the 60 gsm samples. However, the strength doubles between the 360 gsm and 30 gsm or 60 gsm samples. Fig. 1.9 shows the stress-strain curves of the tensile

tests. It can be seen that all configurations have the same stiffness at low strains, as this is mainly dependent on the fibers and their orientation.

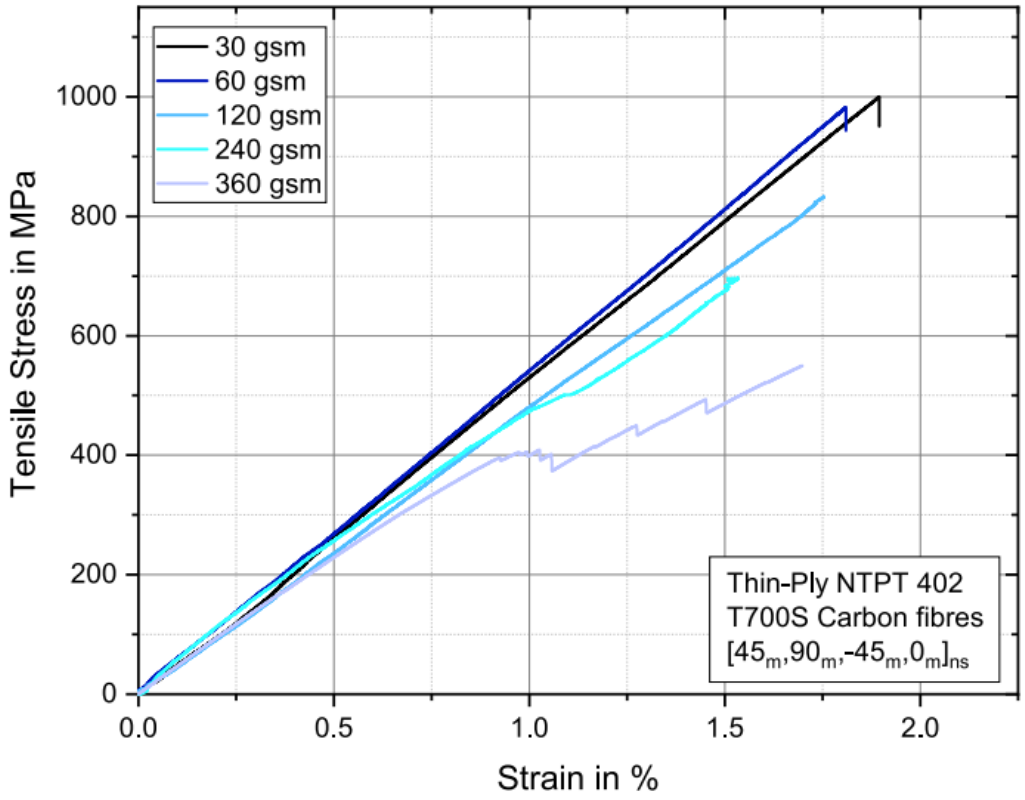

Figure 1.9 – Tensile stress-strain curves depending on the layer thickness

Table 1.3

Number of tested samples for each ply thickness and load

Fiber area weight in gsm					
30		60	120	240	360
Tension	7	6	6	6	5
Compression	6	6	6	6	5
Fatigue R=0.1	20	10	10	_	9
Fatigue R=0.2	19	7	7	_	14
Fatigue R=0.3	10	13	10	_	7
FAI R=0.5	8	6	8	_	5

However, with increasing load, initial damage occurs, and a decrease in stiffness is recorded for thicker layers. Further, samples with thinner layers (30 and 60 gsm) do not show any damage until final failure, and therefore no decrease in stiffness can be determined. The 30 and 60 gsm specimens' fracture patterns show a brittle failure behaviour and exhibit no or almost no delaminations. shows the maximum achievable strength and a reduction of the layer thickness does not offer any further advantage to the mechanical properties investigated. The freedom of design due to the higher number of layers is still an advantage.

Conclusion to the part 1

The first part mainly introduces the application and development of composite structures. Composite materials have high strength, high stiffness, light weight, and other series of advantages such as fatigue resistance, vibration reduction, high temperature resistance, and designability. So, they are widely used in the aerospace field.

With the advent of high-performance fibers such as carbon fiber and boron fiber in the 1960s, the composite is widely used in aircraft structures. At present, the most widely used composite is carbon fiber composite materials.

For composite materials, the different ply thicknesses and ply angles have greater impact on the mechanical properties. As for the research on the properties of thin-layer composite materials. This thesis introduces the researches of composite materials by some scholars from all over the world, and concludes that the composite material laminate shows relatively high resistance to damage and delamination after the thickness of the layer is reduced.

In general, thin-layer composites are superior to conventional ones in terms of mechanical properties and designability, so thin-layer composites have broad development prospects.

PART 2. THEORETICAL BACKGROUND OF COMPOSITE STRUCTURES

Composite materials are made of continuous or discontinuous fibers embedded in a matrix. The directional nature of these fibers in the ply, introduces a directional dependence to the composite layer properties. Materials with direction dependent properties are called anisotropic materials. A special case of anisotropy is the existence of two perpendicular plane of symmetry in the material properties. These materials are classified as orthotropic. The mechanical behavior of composite materials differs from that of isotropic materials, since two directions must be considered for the strength and stiffness properties. This chapter describes how orthotropic composite structural components can be studied using classical laminate (Section 2.1) and thin-walled structures theories (Section 2.3).

A particular characteristic of composite materials is that stiffness and strength properties depend on the direction of the fibers in the laminate. The behavior of these materials, when loaded, is therefore different from isotropic materials and many more parameters must be considered to predict them. This section presents a brief insight on the classical lamination theory to calculate the stiffness properties of composite orthotropic laminates [16].

2.1. Basic mechanics of orthotropic laminates

For unidirectional fiber reinforced lamina, there are two perpendicular planes of symmetry that define the principal axes of the material properties. These principal axes correspond to the direction of the fibers and a direction transverse to the fibers, and are denoted by the subscripts 1and 2 respectively. This coordinate system is a local system associated with the single lamina. A global coordinate system, attached to a fixed reference point, is instead used when the whole laminate is considered, see Figure 2.1.

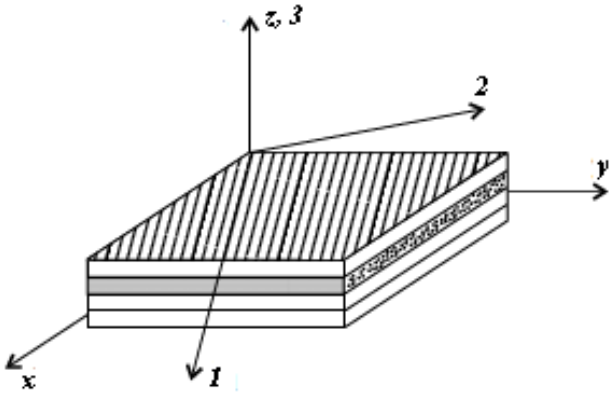

Figure 2.1 – Global and local coordinate system

For a thin orthotropic ply, with no applied forces in the out of plane direction, the stress strain relationship in the principal material direction is defined as:

$$\begin{Bmatrix}\sigma_1\\ \sigma_2\\ \tau_{12}\end{Bmatrix} = \begin{bmatrix}Q_{11} & Q_{12} & 0\\ Q_{11} & Q_{22} & 0\\ 0 & 0 & Q_{66}\end{bmatrix}\begin{Bmatrix}\varepsilon_1\\ \varepsilon_2\\ \gamma_{12}\end{Bmatrix} \tag{2-1}$$

where the Q_{ij}'s are the reduced stiffness and are given in terms of the elastic moduli in the 1 and 2 directions, E_1 and E_2, the shear modulus in the 1-2 plane G_{12}, and the major Poisson's ratio.

$$Q_{11} = \frac{E_1}{1 - v_{12}v_{21}}, \quad Q_{22} = \frac{E_2}{1 - v_{12}v_{21}} \tag{2-2}$$

$$Q_{12} = \frac{v_{12}E_2}{1 - v_{12}v_{21}} = \frac{v_{21}E_1}{1 - v_{12}v_{21}}, \quad Q_{66} = G_{12}$$

The principal Poisson's ratio is defined as the negative ratio of the strain in the 2 direction, e_2, to the strain in the 1 direction, e_1. The minor Poisson's ratio is instead defined as the inverse of the major Poisson's ratio and it is related to the elastic properties through:

$$v_{21} = \frac{E_2}{E_1} v_{12} \tag{2-3}$$

The stresses and strains expressed in the local coordinate system can be transformed to the reference system by using the following relationship:

$$\begin{Bmatrix} \sigma_1 \\ \sigma_2 \\ \tau_{12} \end{Bmatrix} = T \begin{Bmatrix} \sigma_x \\ \sigma_y \\ \tau_{xy} \end{Bmatrix} \text{ and } \begin{Bmatrix} \varepsilon_1 \\ \varepsilon_2 \\ \varepsilon_{12} \end{Bmatrix} = T \begin{Bmatrix} \varepsilon_x \\ \varepsilon_y \\ \varepsilon_{xy} \end{Bmatrix} \tag{2-4}$$

where ε_{xy} and ε_{12} are the tensor shear strain, which correspond to half of the engineering shear strains, γ_{xy} and γ_{12}, and the transformation matrix T is expressed in terms of the sine and cosine of the angle between the axis 1 and x, see Figure 3.1.

$$T = \begin{bmatrix} m^2 & n^2 & 2mn \\ n^2 & m^2 & -2mn \\ -mn & mn & m^2 - n^2 \end{bmatrix}, m = \cos\theta \text{ and } n = \sin\theta \tag{2-5}$$

In order to convert the strain transformation relation from tensor strain to engineering strain, the transformation matrix is pre- and post-multiplied by a matrix R and the inverse of R, where:

$$\begin{Bmatrix} \varepsilon_x \\ \varepsilon_y \\ \gamma_{xy} \end{Bmatrix} = R \begin{Bmatrix} \varepsilon_x \\ \varepsilon_y \\ \varepsilon_{xy} \end{Bmatrix}, R = \begin{bmatrix} 1 & 0 & 0 \\ 0 & 1 & 0 \\ 0 & 0 & 2 \end{bmatrix} \tag{2-6}$$

The transformation matrix for the engineering strains is therefore given by

$$T_e = \begin{bmatrix} m^2 & n^2 & mn \\ n^2 & m^2 & -mn \\ -2mn & 2mn & m^2 - n^2 \end{bmatrix} \tag{2-7}$$

Substituting the transformation matrix T_e for the stresses and engineering strain into Eq. (2-1) the stress-strain relationship in the global coordinate system is expressed as

$$\begin{Bmatrix}\sigma_x\\ \sigma_y\\ \tau_{xy}\end{Bmatrix} = T^{-1}QRTR^{-1}\begin{Bmatrix}\varepsilon_x\\ \varepsilon_y\\ \gamma_{xy}\end{Bmatrix} = \begin{bmatrix}\bar{Q}_{11} & \bar{Q}_{12} & \bar{Q}_{16}\\ \bar{Q}_{12} & \bar{Q}_{22} & \bar{Q}_{26}\\ \bar{Q}_{16} & \bar{Q}_{21} & \bar{Q}_{66}\end{bmatrix}\begin{Bmatrix}\varepsilon_x\\ \varepsilon_y\\ \gamma_{xy}\end{Bmatrix} \tag{2-8}$$

In a laminate with N orthotropic layers perfectly bonded together with an infinitely thin bond line and continuous in-plane deformations across the bond line the strain distribution can be defined as

$$\begin{Bmatrix}\sigma_x\\ \sigma_y\\ \tau_{xy}\end{Bmatrix} = \begin{Bmatrix}\varepsilon_x^0\\ \varepsilon_y^0\\ \gamma_{xy}^0\end{Bmatrix} + z\begin{Bmatrix}\kappa_x\\ \kappa_y\\ \kappa_{xy}\end{Bmatrix} \tag{2-9}$$

where the superscript '0' represents the mid plane strain, and k is the curvature of the laminate. The stresses in the kth ply can be expressed in terms of the reduced stiffness of that particular ply by substituting Eq. (2-9) into the stress-strain relationship Eq. (2-8),

$$\begin{Bmatrix}\sigma_x\\ \sigma_y\\ \tau_{xy}\end{Bmatrix}_{(k)} = \begin{bmatrix}\bar{Q}_{11} & \bar{Q}_{12} & \bar{Q}_{16}\\ \bar{Q}_{12} & \bar{Q}_{22} & \bar{Q}_{26}\\ \bar{Q}_{16} & \bar{Q}_{21} & \bar{Q}_{66}\end{bmatrix}_{(k)}\left(\begin{Bmatrix}\varepsilon_x^0\\ \varepsilon_y^0\\ \gamma_{xy}^0\end{Bmatrix} + z\begin{Bmatrix}\kappa_x\\ \kappa_y\\ \kappa_{xy}\end{Bmatrix}\right) \tag{2-10}$$

The laminate in-plane forces and moments per unit width applied to a point in the laminate are obtained by through thickness integration of the stresses in each ply

$$\begin{Bmatrix}N_x\\ N_y\\ N_{xy}\end{Bmatrix} = \int_{-h/2}^{h/2}\begin{Bmatrix}\sigma_x\\ \sigma_y\\ \tau_{xy}\end{Bmatrix}dz, \quad \begin{Bmatrix}M_x\\ M_y\\ M_{xy}\end{Bmatrix} = \int_{-h/2}^{h/2}\begin{Bmatrix}\sigma_x\\ \sigma_y\\ \tau_{xy}\end{Bmatrix}_{(k)} zdz \tag{2-11}$$

Substituting the stress-strain relationship of Eq. (2-10) into Eq. (2-11) the following constitutive relation for the laminate can be defined

$$\begin{Bmatrix} N_x \\ N_y \\ N_{xy} \\ M_x \\ M_y \\ M_{xy} \end{Bmatrix} = \begin{bmatrix} \begin{bmatrix} A_{11} & A_{12} & A_{16} \\ A_{12} & A_{22} & A_{26} \\ A_{16} & A_{26} & A_{66} \end{bmatrix} & \begin{bmatrix} B_{11} & B_{12} & B_{16} \\ B_{12} & B_{22} & B_{26} \\ B_{16} & B_{26} & B_{66} \end{bmatrix} \\ \begin{bmatrix} B_{11} & B_{12} & B_{16} \\ B_{12} & B_{22} & B_{26} \\ B_{16} & B_{26} & B_{66} \end{bmatrix} & \begin{bmatrix} D_{11} & D_{12} & D_{16} \\ D_{12} & D_{22} & D_{26} \\ D_{16} & D_{26} & D_{66} \end{bmatrix} \end{bmatrix} \begin{Bmatrix} \varepsilon_x^0 \\ \varepsilon_y^0 \\ \gamma_{xy}^0 \\ \kappa_x \\ \kappa_y \\ \kappa_{xy} \end{Bmatrix} \tag{3-12}$$

where [A], [B], and [D] matrices are the laminate stiffness matrix and are defined in terms of the ply stiffness as

$$\begin{aligned} A_{ij} &= \sum_{k=1}^{N} \left(\bar{Q}_{ij}\right)_{(k)} (z_k - z_{k-1}) \\ B_{ij} &= \frac{1}{2} \sum_{k=1}^{N} \left(\bar{Q}_{ij}\right)_{(k)} \left(z_k^2 - z_{k-1}^2\right) \\ D_{ij} &= \frac{1}{3} \sum_{k=1}^{N} \left(\bar{Q}_{ij}\right)_{(k)} \left(z_k^3 - z_{k-1}^3\right) \end{aligned} \tag{2-13}$$

The matrices [A] and [D] represent the laminate membrane and bending stiffness respectively while the matrix [B] represents the coupling stiffness. These three matrices therefore, determine the stiffness of a laminate in different directions and describe the response of a laminate to in-plane forces and moments.

2.2. Composite laminates design principles

The mechanical properties of epoxy carbon are mainly determined by its ply design. The lay-up design of laminates mainly includes three aspects: firstly, selecting the appropriate single-layer laying angle; secondly, determining the number of layers at each laying angle, that is, the laying ratio; finally, determining the laying order. The layup design of laminates generally follows the following principles:

(1) Balanced and symmetrical laying principle

Except for special needs, the structures are generally designed in the form of balanced and symmetrical laminates to avoid warping deformation after curing caused by tension-shear and tension-bending coupling.

(2) The principle of lay-up orientation

In the case of satisfying the force, the number of laying directions should be as few as possible to simplify the workload of design and construction. Generally, 4 layup directions such as 0°, 90° and ±45° are selected.

(3) Layer orientation is selected according to the principle of load bearing

The fiber axial direction of the layup should be consistent with the tension and compression direction of the internal force to maximize the high performance of the fiber axial direction.

(4) Principle of laying sequence

It is mainly considered from three aspects: each directional single layer should be distributed as evenly as possible along the thickness of the laminate, and the layers at the same corner should be avoided. If necessary, no more than 4 layers are generally used to reduce cracking and edge delamination of both orientation layers. In addition, the laying sequence has a great influence on the stability and bearing capacity of the laminate, and this factor should also be considered.

(5) The principle of minimum proportion of layers

In order to make the matrix of the composite material unloaded in all directions, for a laminate composed of layers with directions of 0°, 90°, and ±45°, the minimum layer ratio in any direction should be ≥6%~10%.

(6) Design principles of impact load zone

For laminates that are impacted by concentrated in-plane forces, local reinforcement is required. In addition, local reinforcement measures need to be taken to ensure sufficient strength.

(7) Design principles of connecting area

The ratio of the layup at ±45° to the nail loading direction should be ≥40%, and the ratio of the layup consistent with the nail loading direction should be greater than 25% to

ensure that the connection area has sufficient shear strength and extrusion strength, and is also conducive to Diffuse loads and reduce stress concentrations in pores.

(8) Design principles of variable thickness

In the area of variable thickness of the structure, the increase or decrease of the number of layers should form a gradual change of steps, because the sudden change of thickness will cause stress concentration. The width of each step is required to be similar and ≥60°, and the height of the step should not exceed 1/10 of the width. A continuous cover layer is then applied to the surface to prevent delamination damage outside the steps.

(9) Laying principle of open area

In the opening area of the structure, the included angle of the adjacent layers should be ≤60° to reduce the interlayer stress. The shape of the opening should use a round hole as much as possible, because the stress concentration on the edge of the round hole is small. If rectangular holes must be used, rounded corners with larger radii should be used at the corners. In addition, when opening, the fiber should be cut as little as possible [17].

2.3. Stress-strain analysis of thin-walled section beams

An aircraft can be considered as an assembly of panels ranging from open to multicell closed sections subject to bending, shear, torsional and axial loads. Because the thickness of these panels is small compared to the cross-sectional dimensions, these structures are often treated as thin-walled beams. Exploiting the thin-walled nature of aircraft structures simplifying assumption can be made when calculating stresses and displacements. The stress across the thickness of the plates can in fact be considered constant and furthermore the squares and higher order power of the thickness term can be neglected when computing the sectional properties. A detailed analysis of open and closed isotropic thin-walled beams under various types of loadings can be found in [18]. In this section however composite thin-walled structures are considered and the methods to analyze the behavior of open and closed section beams under bending and torsion are shown.

The stresses due to the bending moments MX and MY are calculated in the same manner for both closed and open sections. These moments are taken to be positive when

each induces a tensile stress in the positive XY quadrant of the GXY axis system. G is the centroid of the section and passes through the neutral axis of the section NA. The neutral axis is inclined at an angle α with respect to the X-axis. Each laminate x-axis is parallel to the global Z-axis.

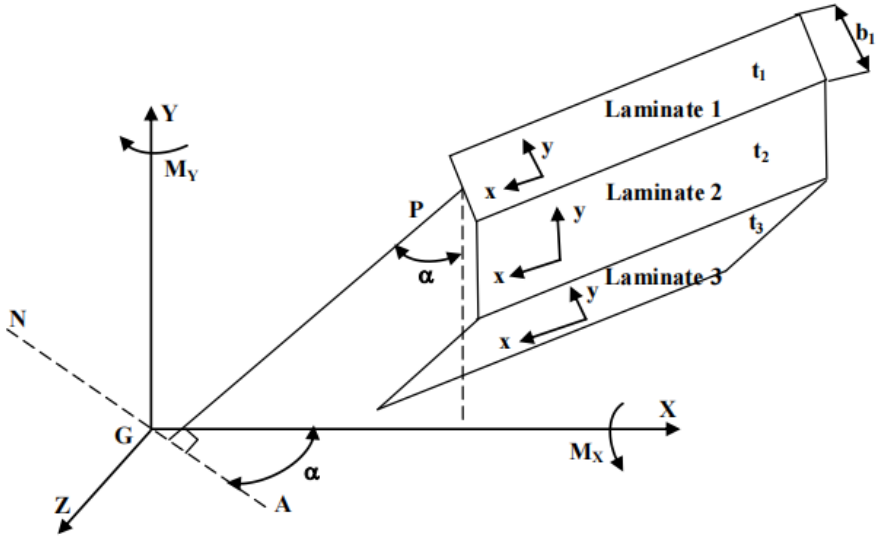

Figure 2.2 - Global and local coordinate system for an arbitrary section under bending loads

The analysis is carried out by first considering each panel separately, for example the Laminate 1 with thickness t_1 and a small element of area A is selected, see Figure 2.2. This area is at a distance P from the neutral axis and it is defined as

$$P = X\sin\alpha + Y\cos\alpha \tag{2-14}$$

The direct stress σ_z, on the element area δA, at a distance P from the neutral axis is given by the expression

$$\sigma_Z = E_Z \frac{P}{R} \tag{2-15}$$

where Ez is the elastic modulus in the global Z-direction and R is the radius of the curvature at the section. Since the Z-axis and laminate x-axis are parallel the stresses and the elastic modulus in the global Z-direction can be defined as

$$\sigma_Z = \sigma_x, \quad E_Z = E_x \tag{2-16}$$

Substituting the expression for P from Eq. (2-14) into Eq. (2-15) the following relationship is obtained

$$\sigma_Z = \frac{E_Z}{R}(X\sin\theta + Y\cos\theta) \tag{2-17}$$

The resultant moments M_X and M_Y are given by the expressions

$$M_X = \int_A \sigma_Z Y dA$$

$$M_Y = \int_A \sigma_Z X dA \tag{2-18}$$

Where A is the area integration limits for the panel considered. Substituting Eq. (2-17) into Eq. (2-18) the expression for the moment forces can be rewritten as

$$M_X = \int_A \frac{E_Z}{R}(X\sin\alpha + Y\cos\alpha)Y dA$$

$$M_Y = \int_A \frac{E_Z}{R}(X\sin\alpha + Y\cos\alpha)X dA \tag{2-19}$$

or by expanding

$$M_X = \frac{\sin\alpha}{R} E_Z \int_A X\,Y dA + \frac{\cos\alpha}{R} E_Z \int_A Y^2\, dA$$

$$M_Y = \frac{\sin\alpha}{R} E_Z \int_A X^2\, dA + \frac{\cos\alpha}{R} E_Z \int_A X\,Y dA \tag{2-20}$$

However the integral terms are by definition the cross sectional properties of the beam.

$$\begin{aligned} \int_A X\,Y dA &= I_{XY} \\ \int_A Y^2\, dA &= I_{XX} \\ \int_A X^2\, dA &= I_{YY} \end{aligned} \tag{2-21}$$

Eq. (2-20) therefore becomes

$$M_X = \frac{\sin\alpha}{R} E_Z I_{XY} + \frac{\cos\alpha}{R} E_Z I_{XX}$$

$$M_Y = \frac{\sin\alpha}{R} E_Z I_{YY} + \frac{\cos\alpha}{R} E_Z I_{XY} \tag{2-22}$$

Remembering that $E_Z = E_X$ and that E_Z is likely to vary from each laminate, the cross-sectional properties can be redefined to include the effective elastic modulus in the member Z-direction as

$$\begin{aligned} I'_{XY} &= E_Z I_{XY} \\ I'_{XX} &= E_Z I_{XX} \\ I'_{YY} &= E_Z I_{YY} \end{aligned} \tag{2-23}$$

Substituting Eq. (2-23) into Eq. (2-22) the expressions for bending moments become:

$$M_X = \frac{\sin\alpha}{R} I'_{XY} + \frac{\cos\alpha}{R} I'_{XX}$$

$$M_Y = \frac{\sin\alpha}{R} I'_{YY} + \frac{\cos\alpha}{R} I'_{XY} \quad (2\text{-}24)$$

Solving the two expressions in Eq. (2-24) simultaneously it is obtained that

$$\frac{\sin\alpha}{R} = \frac{M_Y - M_X I'_{XY}/I'_{XX}}{I'_{YY}(1 - {I'_{XY}}^2/I'_{XX}I'_{YY})} = \frac{M'_Y}{I'_{YY}}$$

$$\frac{\cos\alpha}{R} = \frac{M_X - M_Y I'_{XY}/I'_{YY}}{I'_{XX}(1 - I'_{XY}/I'_{XX}I'_{YY})} = \frac{M'_X}{I^X_{XX}} \quad (2\text{-}25)$$

Where $M'_Y = \frac{M_Y - M_X I'_{XY}/I'_{XX}}{(1 - {I'_{XY}}^2/I'_{XX}I'_{YY})}$

$M'_X = \frac{M_X - M_Y I'_{XY}/I'_{YY}}{(1 - {I'_{XY}}^2/I'_{XX}I'_{YY})}$

Substituting Eq. (2-25) into Eq. (2-17) the following expression for stress is obtained

$$\sigma_Z = E_Z \left(\frac{M'_Y}{I'_{YY}} X + \frac{M'_X}{I'_{XX}} Y \right) \quad (2\text{-}26)$$

σ_Z is therefore the normal stress acting on the Laminate 1 in the beam Z-direction due to the applied moments M_X and M_Y. The axial force intensity on the Laminate 1 is given by

$$N_x = \sigma_x t \quad (2\text{-}27)$$

where t is the laminate thickness.

When all the n laminates of the section are considered, the sectional properties become

$$\begin{aligned} I'_{XY} &= \sum_{i=1}^{n}(E_Z I_{XY})_i \\ I'_{XX} &= \sum_{i=1}^{n}(E_Z I_{XX})_i \\ I'_{YY} &= \sum_{i=1}^{n}(E_Z I_{YY})_i \end{aligned} \qquad (2\text{-}28)$$

The direct stresses at a point in the laminate due to bending moments can then be obtained using Eq. (2-26) by substituting the value of EZ of the considered laminate.

Studying the strength of materials is a very complex process because it is related to many factors that contribute to failure. Strength is not only due to the inherent properties of the material itself, but also depends on the environmental factors and loading conditions in which the material is exposed. Because the composite material is an anisotropic composite, the properties, content, orientation and interfacial bonding state of its component materials all affect its strength, so the strength issues involved in the composite material are quite complicated. This section will not discuss its failure mechanism, but only introduce the more widely used failure criteria in composite structure design, including: Tsai-Hill criterion, Tsai-Wu criterion, Hoffman criterion [19,20].

The Tsai-Hill strength criterion is an extension of the von Mises yield criterion for isotropic materials in orthotropic materials. Mises' yield criterion is

$$(\sigma_y - \sigma_z)^2 + (\sigma_z - \sigma_x)^2 + (\sigma_x - \sigma_y)^2 + 6(\tau_{yz}^2 + \tau_{zx}^2 + \tau_{xy}^2) < 2\sigma_s^2 \qquad (2\text{-}29)$$

where σs is the yield stress of uniaxial tension. If it occurs in a plane stress state, it can be written in the following form.

$$\sigma_x^2 + \sigma_y^2 - \sigma_x\sigma_y + 3\tau_{xy}^2 < \sigma_s^2 \qquad (2\text{-}30)$$

When the yield failure of the material under the action of pure shear stress also satisfies (2-29), the pure shear yield stress $\tau_s = \sigma_s/\sqrt{3}$ is obtained, which is substituted into the above formula (2-30) to obtain

$$\frac{\sigma_x^2}{\sigma_s^2}+\frac{\sigma_y^2}{\sigma_s^2}-\frac{\sigma_x\sigma_y}{\sigma_s^2}+\frac{\tau_{xy}^2}{\tau_s^2}<1 \qquad (2\text{-}31)$$

The Tsai-Hill criterion holds that: referring to the above formula, the following formula can be used as the strength condition of the single-layer orthotropic composite material.

$$\frac{\sigma_1^2}{X^2}+\frac{\sigma_2^2}{Y^2}-\frac{\sigma_1\sigma_2}{X^2}+\frac{\tau_{12}^2}{S^2}<1 \qquad (2\text{-}32)$$

The above formula (2-32) is the Tsai-Hill criterion. It should be noted that the Tsai-Hill criterion can in principle only be used for composite monolayers where the tensile and compressive strengths of the material in the principal elastic direction are the same (Xc = Xt = X, Yc = Yt = Y). If it is a material with different tensile and compressive strengths, then the tensile strength Xt is used for the tensile stress σ1, and the tensile strength Yt is used for the tensile stress σ2; the compressive strength Xc is used for the compressive stress σ1, and the compressive strength Yc is used for the compressive stress σ2. The Tsai-Hill criterion links the three stresses in the principal directions of a single-layer material and the corresponding basic strengths in one expression, taking into account their mutual influences. If the inequality of the above formula (2-32) is not satisfied, the material will fail; to ensure the normal operation of the material, the sum of the terms on the left side of the inequality must be less than 1.

The Hoffman strength criterion modified the Tsai-Hill criterion. He did not consider the influence of the material failure by the different tensile and compressive strengths of a single layer, and added the odd function terms of σ1 and σ2, and then proposed the following Hoffman Fulman strength criterion.

$$\frac{\sigma_1^2-\sigma_1\sigma_2}{X_tX_c}+\frac{\sigma_2^2}{Y_tY_c}+\frac{X_c-X_t}{X_tX_c}\sigma_1+\frac{Y_c-Y_t}{Y_tY_c}\sigma_2+\frac{\tau_{12}^2}{S^2}<1 \qquad (2\text{-}33)$$

Therefore, the material failure is affected by the different tensile and compressive strengths of a single layer, which can be reflected by the first-order terms of σ1 and σ2 in Eq. (2-33). The Tsai-Hill criterion is derived from the above formula when Xc = Xt and Yc = Yt.

Tsai-Wu tensor criterion: The above strength criteria are not perfect. For this reason, Stephen W. Tsai and Edward M. Wu proposed a new strength criterion, which is based on Expression in tensor form.

$$F_{11}\sigma_1^2 + 2F_{12}\sigma_1\sigma_2 + F_{22}\sigma_2^2 + 2F_{16}\sigma_1\sigma_6 + 2F_{26}\sigma_2\sigma_6 + F_1\sigma_1 + F_2\sigma_2 + F_6\sigma_6 < 1 \quad (2\text{-}34)$$

where: $F_{11} = \frac{1}{X_t X_c}$, $F_{22} = \frac{1}{Y_t Y_c}$, $F_{66} = \frac{1}{S^2}$, $F_1 = \frac{1}{X_t} - \frac{1}{X_c}$, $F_2 = \frac{1}{Y_t} - \frac{1}{Y_c}$. When F_{12}= 0, the calculation results of Tsai-Wu tensor criterion and Hoffman strength criterion are similar. When $F_{12} = \sqrt{F_{11}F_{22}}/2$, the theoretical value is in agreement with the experimental value well.

2.4. Model selection and analytical solution

To achieve structural weight reduction on the premise of ensuring the structural bearing capacity is the tireless pursuit of the aerospace field. Carbon fiber composite materials and their structures are favored by aircraft designers due to their excellent mechanical properties and weight reduction effects, and has been widely used in the aerospace field.

Aircraft wings today share the same basic design are shown in figure 2.3. The purpose of the wing of course is to produce lift, achieved by creating a higher-pressure airflow under the wing, and lower above the wing. This is caused by the curvature of the aero-foil, guiding the design of all wings.

Figure 2.3 – Basic design of aircraft wings

As the main component for providing flight lift, the wing has the characteristics of large aspect ratio (span²/wing area) and wingspan. At the same time, it requires high structural rigidity and strength, and great adaptability to the flight environment. In addition, in terms of weight, the requirement for structural lightweight is significant. The ratio of structural weight to effective load can only be guaranteed if the structural weight factor is small enough. Therefore, modern aircraft have chosen high-performance carbon fiber composite materials.

How to ensure that wings with the large aspect ratio and the large aspect ratio has sufficiently high structural rigidity and structural weight as light as possible is difficult challenge for structural design. In the wing structure, the wing main spar is the most important bearing part. Therefore, the design of the wing main spar (fig.2.4) has become the key to facing challenges and solving problems.

This paper takes "A350-800" as a reference, which with the maximum take-off 248,000 kg, the wingspan of 64.75 m [21]. The ultimate A350 wings flex is 5 m [22]. The wings are of metal-ribbed, three-spar, carbon fiber reinforced plastic (CFRP) construction [23]. The A350's C-section spar's three segments average 10m/32 ft in length [24], with a thickness of 25 mm/0.08 ft at the root end(T0), which tapers to just 5 mm/0.020 inch at the wing tip(T1) of the outermost segment [25].

Figure 2.4 – A350 spar

For the convenience of simulation, this paper will simplify the spar. Assuming that, the thickness of the tapered spar follows this equation:(L is the full-length spar).

$$T=0.025-L/1,500 \tag{2-35}$$

The height of the spar at the root end is nearly 2m/6.5 ft and tapers to about 0.25m/10 inches at the wingtip [24]. Assuming that the heights of the tapered spar follow this equation:

$$H=2-(1.75/30)*L \tag{2-36}$$

The root spar section weighs about 500 kg with composite laminates up to some 25-30 mm thick. The mid-section, which has many attachment points, weighs about 150 kg, while the outboard section weighs 100 kg [26].

The ultimate load is calculated as 2.5 times the maximum expected G load that the aircraft would ever encounter in its service life. For the Airbus A350, which is limited in the G loads that it may experience, by the Fly by Wire system to +2.5G, or with the FBW system deactivated, as is the case with a reversion to direct law, approximately between 3-3.5G with the aerodynamic limitations of the flight control surfaces. The ultimate load is then possibly

between 7.5 – 8.75G [23], for the convenience of calculation, it is assumed that the sum of other external forces on the aircraft is equal to the maximum take-off gravity (about 2430400 N) and choosing the ultimate load as 8 G, then we can get the ultimate load is 19,443,200 N, most of the loads acting on the wings (assuming as 18,000,000N). Assuming that six spars are same, then each spar carry the ultimate load is 3000000 N. This paper selects the root spar (Weight=500 kg) as the research object. In accordance of the shape of the spar, which can be simply regarded as non-uniform distribution of force(F) acting on each spar. And I searched about that the Epoxy Carbon with 24 mm thickness can hold 168,000N, for the convenience of simulation, we can assume that the ultimate load of Epoxy Carbon with 25mm thickness is 175,000 N, ultimate load of 5mm thickness is 25,000 N. Assuming that the force on the spar is continuous uneven distribution, then we can get:

$$F=175,000-5,000*L \tag{2-37}$$

About the relationship between the wing flex(X) and length can be seen like:

$$X=5*L/30 \tag{2-38}$$

Their size and weight is difficult to convey in words and dimensions, so the main beam is simplified. About the cap length of spar, according to the literature reviewed, assuming that the cap of root end is 0,5m, the cap of wingtip is 0.1m. And about the length of cap follows this equation:

$$L(c)=0.5-L/75 \tag{2-39}$$

Conclusion to the part 2

This chapter introduces the basics of composite mechanics: stiffness analysis of laminates using classical laminate theory, thin-walled structures theories, several commonly used composite structural strength criteria and the model selection. Prepared theoretical knowledge for the design and finite element analysis of composite spars in the next chapter.

PART 3. CONCEPTUAL DESIGN OF THE WING SPAR

3.1 The main beam of the wing structure

The spar is the main longitudinal force-bearing member of the wing, which mainly bears the shear force and bending moment. However, due to the uneven force on the wing, there will also be torque generated. Aerodynamic lift loads acting on the top and bottom surfaces of the wing are transferred to the rib structure, which in turn is transferred to the spar web in the form of concentrated shear loads. These shear loads cause the spar to bend, which is the dominant load on the spar. In addition, fuel load inertia loads as well as engine accessory loads are also transferred to the spars. The multiple transitions to several spars to concentrate all aerodynamic loads and then transmit them to the fuselage. For this chapter, the effect of the bending moment on the spar is mainly studied, because the load of the aircraft is mainly reflected in the bending moment of the spar. Under the condition that the spar bending resistance is satisfied, other factors will be considered.

Most of the wings of large aircraft adopt wing box structure layout, and the wing box adopts a composite material skin reinforcement structure, and they often use beams in the form of "I", "C" and "π" shapes (as shown in the figure 3.1).

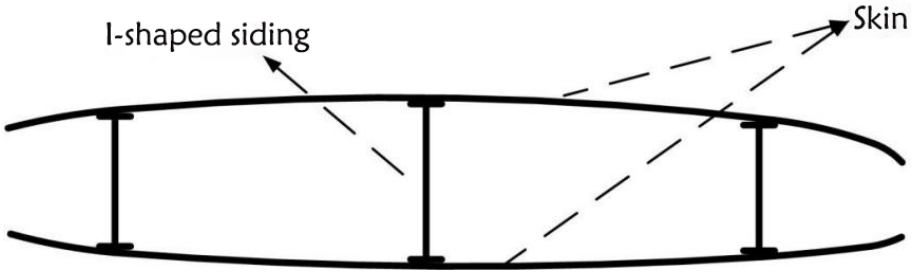

(a) I-shaped wing box

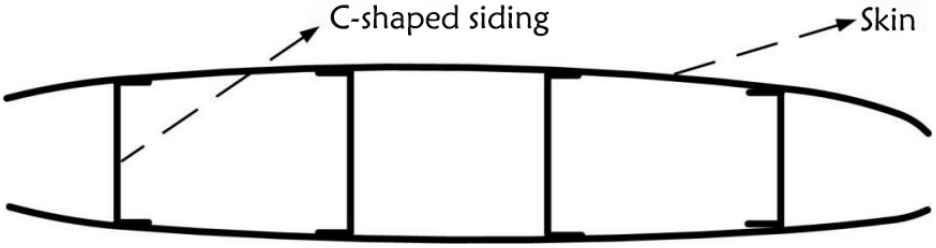

(b) I-shaped wing box

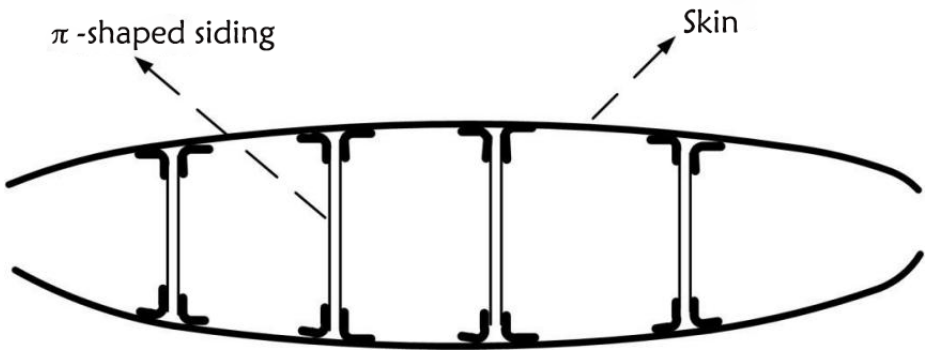

(c) π - shaped wing box

Figure 3.1 – Wing box consisting of skin and (a) I-shaped, (b) C-shaped and (c) π-shaped spars

The Airbus A350 wing adopts "C"-shaped structure. The A350 front spar is about 32 meters [27]. The GKN Aerospace (Filton, U.K.) factory in the Western Approach of the U.K. is dedicated to wing spar manufacturing. It produces the rear spar for the Airbus A350 [28].

3.2 Wing spar models and their stress-strain analysis

Nowadays, the internal arrangement of the wing. In order to improve the structural efficiency and make full use of the wing space, the wings of modern aircraft generally use the structure of the wing itself to arrange the fuel tank of the overall structure of the wing. For this reason, some special problems must be solved in the structure. In addition, whether the landing gear needs to be fixed or stored on the wing, whether the engine or other external suspension is installed, and the connection relationship with the front and rear edge movable surfaces, etc., will have a direct impact on the layout of the wing force components. When we choose the wing spar, we need to consider the space occupied by wing spars. But for truss structure one of the most important disadvantages is that it requires a lot of space because the interconnected triangular components must be large to withstand and distribute heavy loads.

This chapter only compares load-bearing performance of C-spar, I-spar, box-spar and tube-spar.

In this chapter, all spars with same height (2 m), same diameter of circumcircle of section (2061.55 mm), same thickness of cap (flange) and web (25 mm), same length (10m), same length of cap (0.5 m).

Figure 3.2 shows the geometric design of the C-spar, I-spar, Box-spar, Tube-spar:

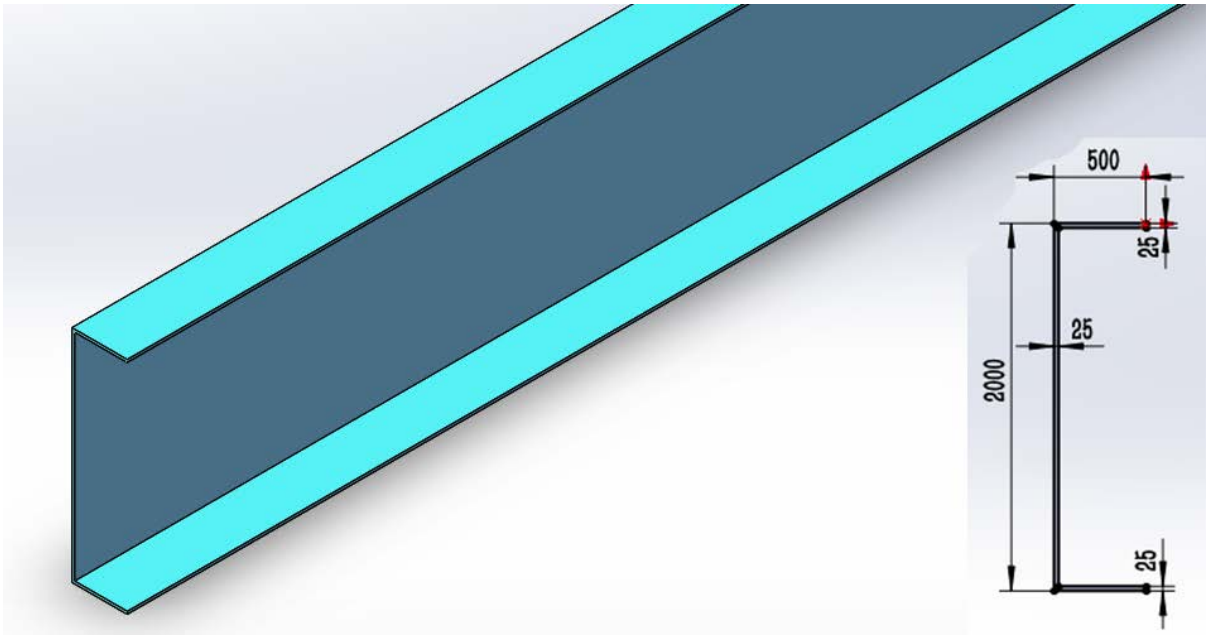

(a) Geometric design of C-spar

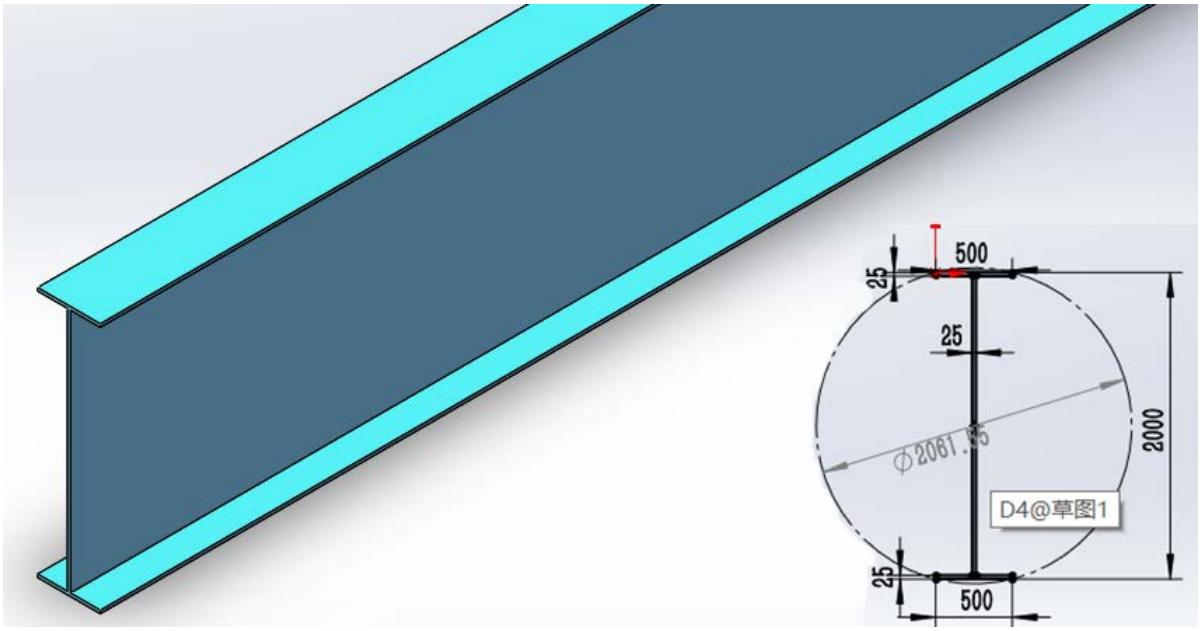

(b) Geometric design of I-spar

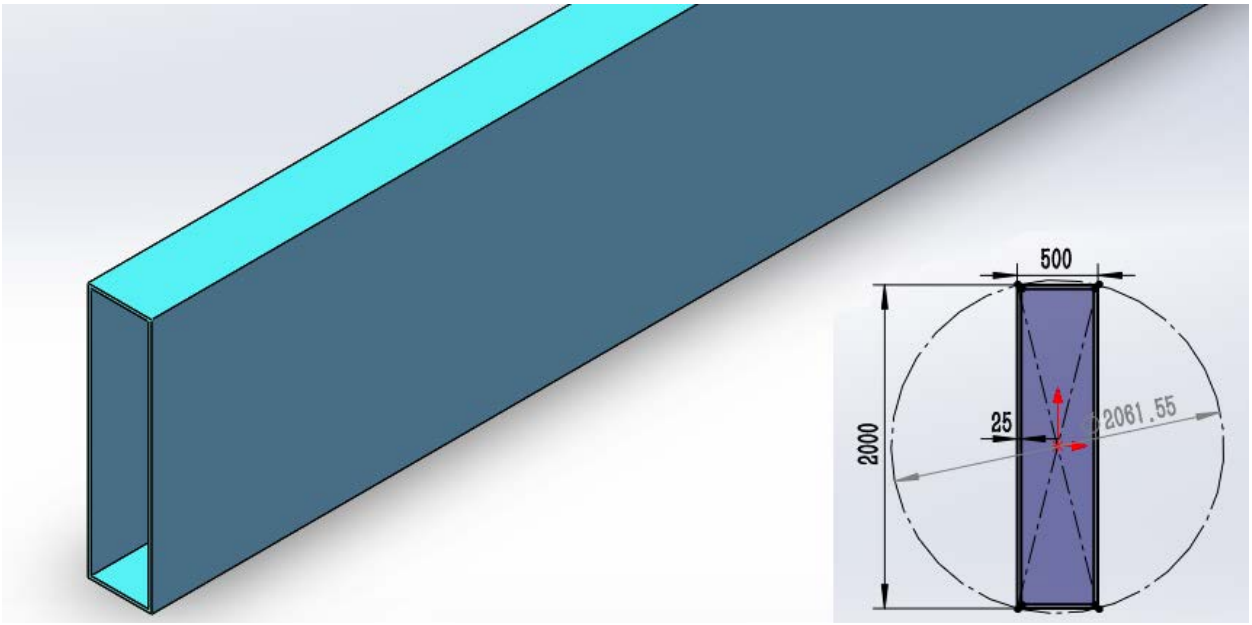

(c) Geometric design of box-spar

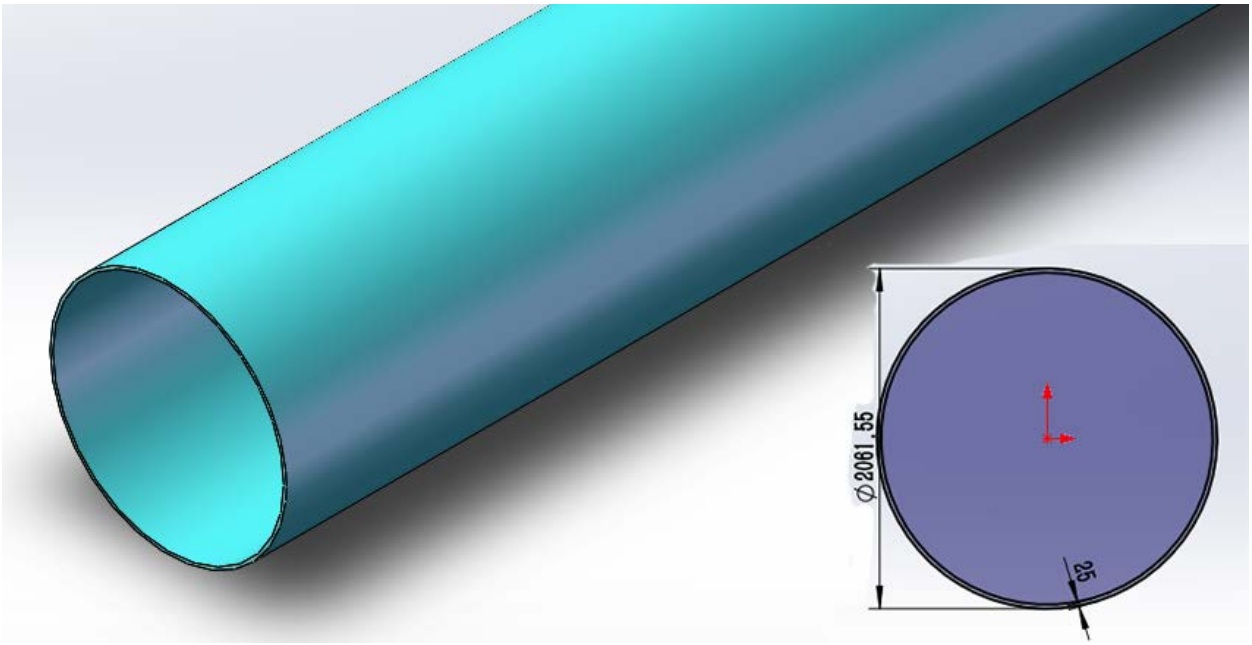

(d) Geometric design of tube-spar

Figure 3.2 – The geometric design of the C-spar, I-spar, Box-spar, Tube-spar

In the design process of the spar of the above four configurations, the material performance parameters of Al 7075-T6 used in the simulation calculation are shown in Table 3.1.

Table 3.1

Mechanical properties of the Al 7075-T6

Density	2810 kg/m³
Young's Modulus	7.17E+10 Pa
Poisson's Ratio	0.33
Shear Modulus	2.69E+10 Pa
Tensile Strength	5.7E+8 Pa
Yield Strength	5.05E+8 Pa

Importing the C-spar, I-spar, box-spar, tube-spar models into Ansys, applying Al 7075-T6 as their material to do simulation about total deformation, equivalent stress. About their masses are presented in table 3.2:

Table 3.2

Masses of the presented types of the spar

C-spar	2072.4 kg/m³
I-spar	2072.4 kg/m³
Box-spar	3442.2 kg/m³
Tube-spar	4494.6 kg/m³

According to the design data, we can get the total force on this spar is 1,750,000 N, applying this force on spar to do simulation.

Figure 3.3 shows the total deformation of C-spar, minimum deformation 0 m, maximum deformation is 1.1837 m, average deformation 0.28389 m.

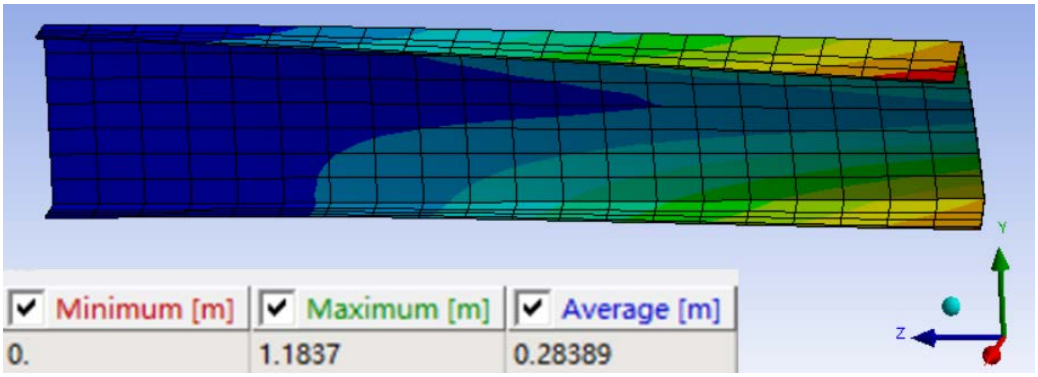

Fig 3.3 – Total deformation of C-spar

Figure 3.4 shows the equivalent stress of C-spar, minimum equivalent stress 1.5193 MPa, maximum equivalent stress is 0.95655 GPa, average equivalent stress 0.18657 GPa.

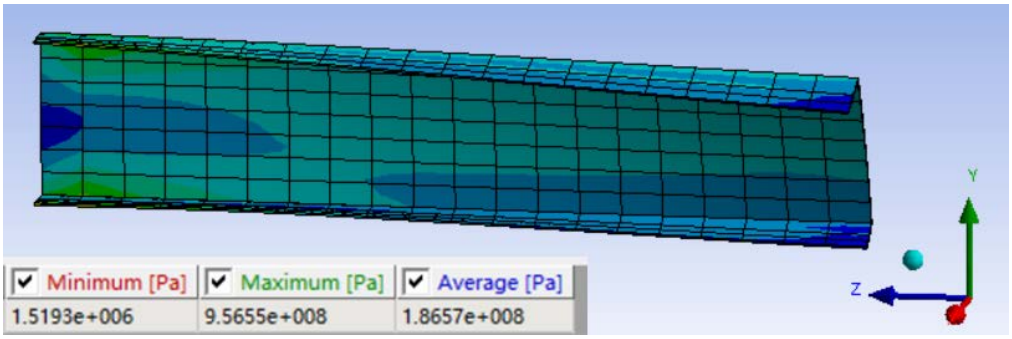

Fig 3.4 – Equivalent stress of C-spar

Similarly, we can obtain the total deformation and equivalent stress of the other three spars, all parameters can be presented in table 3.3:

Table 3.3

Total deformation and equivalent stress of C-spar, I-spar, box-spar and tube-spar

Parameters Spars	Minimum deformation (m)	Maximum deformation (m)	Average deformation (m)	Minimum Equivalent stress (MPa)	Maximum Equivalent stress (GPa)	Average Equivalent stress (GPa)
C-spar	0	1.1837	0.28389	1.5193	0.95655	0.18657
I-spar	0	0.085321	0.03631	0.29069	0.22815	0.067602
Box-spar	0	0.065576	0.027218	0.99734	0.22345	0.052995
Tube-spar	0	0.04118	0.01772	0.056931	0.14219	0.014219

Combining Tables 3.2 and 3.3, C-spar performed the worst. I-spar and tube-spar performed best. Box-spar compares with I-spar, box-spar is 66% heavier than I-spar, but only 30% more resistant to maximum deformation than I-spar. As for the maximum equivalent stress, it is almost the same as the I-spar. In addition, from the simulation, box-spar also does not have the ability to resist torsion, which has poor stability like C-spar.

Next, I-spar and tube-spar will be compared when they have same mass. By calculation, when the weight of tube-spar is the same as I-spar, the wall thickness is about 11.53 mm and the mass is 2086.6 kg.

Figure 3.5 shows the total deformation of C-spar, minimum deformation 0 m, maximum deformation is 0.087851 m, average deformation 0.03786 m.

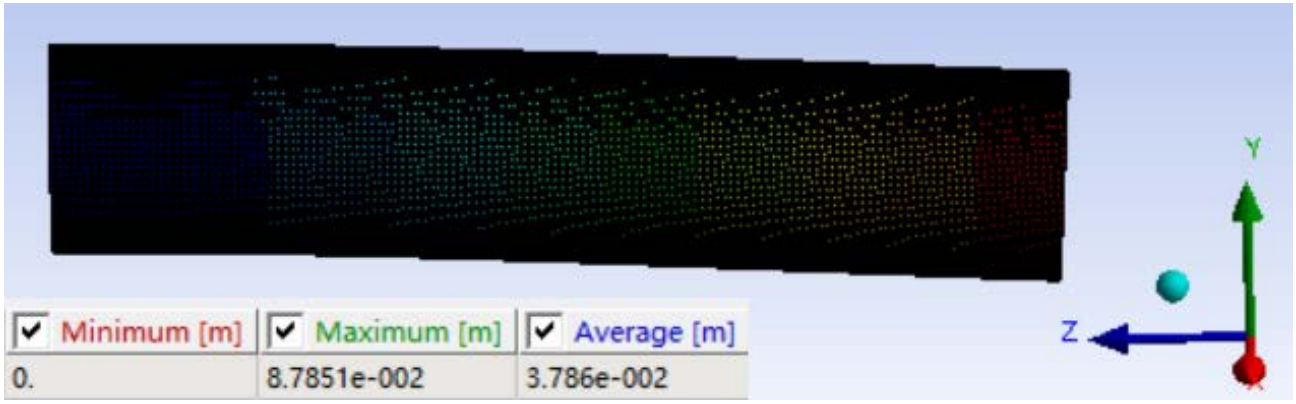

Fig 3.5 – Total deformation of tube-spar

Figure 3.6 shows the equivalent stress of C-spar, minimum equivalent stress 0.0498 MPa, maximum equivalent stress is 0.27009 GPa, average equivalent stress 0.06115 GPa.

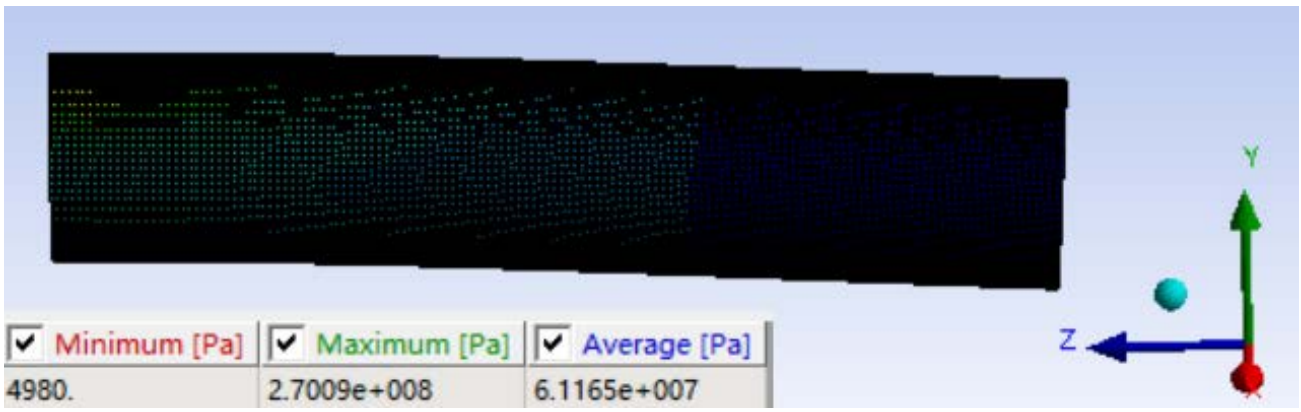

Fig 3.6 – Equivalent stress of tube-spar

The total deformation and equivalent stress of I-spar and tube-spar, all parameters can be presented in table 3.4, which shows that the mechanical properties of I-spar are slightly better.

Table 3.4

Total deformation and equivalent stress of I-spar and tube-spar

Parameters / Spars	Minimum deformation (m)	Maximum deformation (m)	Average deformation (m)	Minimum Equivalent stress (MPa)	Maximum Equivalent stress (GPa)	Average Equivalent stress (GPa)
I-spar	0	0.085321	0.03631	0.29069	0.22815	0.067602
Tube-spar	0	0.087851	0.03786	0.0498	0.27009	0.06115

But from the perspective of wing installation and the space occupied by the spar, tube-spar is not easy to install and takes up a lot of space. So in the wing design, I-spar is better than tube-spar.

In modern aircraft design, weight reduction is one of the key points of aircraft design. As shown in table 2.2, figure 2.4 and figure 2.5, the C-spar does not have any advantages over other types of spars, except for its light weight. On the contrary, I-spar performed the best overall. Therefore, under comprehensive consideration, I-shaped spar are the most suitable for the design requirements. But Boeing 787 and Airbus 350 both chose C-shaped wing spar, the C-spar must have its advantages under the condition that the torque is balanced. This chapter will study it.

It can be seen from the figure 3.7, wing rib plays a vital role on the geometry, shape and the construction of the aircraft wing structure. Wing ribs are in the form of aero-foils and impart required shape to the wing. Wing ribs are also used to reduce the length of the stringers. they are used to support the skin-stringer combination. In wing design, single C-spar is insufficient in torsion resistance. In order to better reflect the advantages of C-spar, it will be verified by means of using symmetric C-spar and supports (their functions like

ribs) to balance the torque. Next, we will investigate the comprehensive mechanical properties of C-spar and I-spar under the same support conditions.

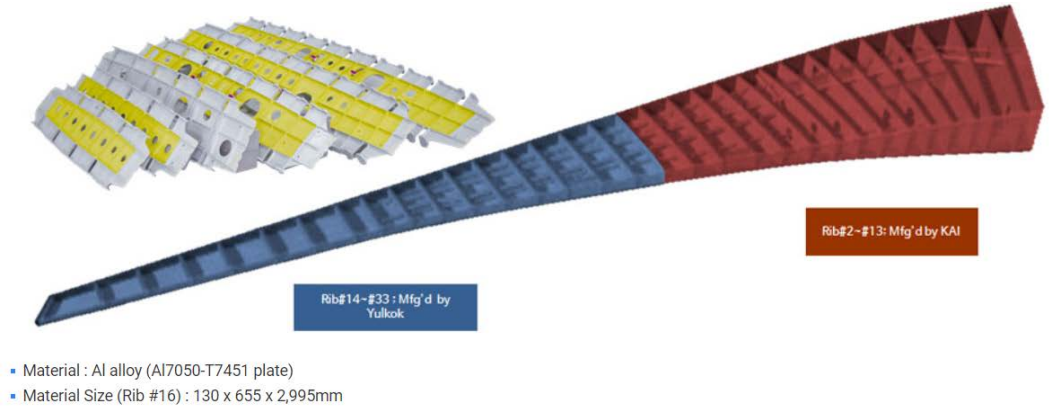

Figure 3.7 – The layout of Spars and Ribs

In order to simulate the function of ribs as much as possible, 25mm thick support plates are selected for support. The form of support is shown in the figure 3.8. Ten 25 mm thick support plates, the distance between each plate is 1.1 m. The same as the support of I-spar.

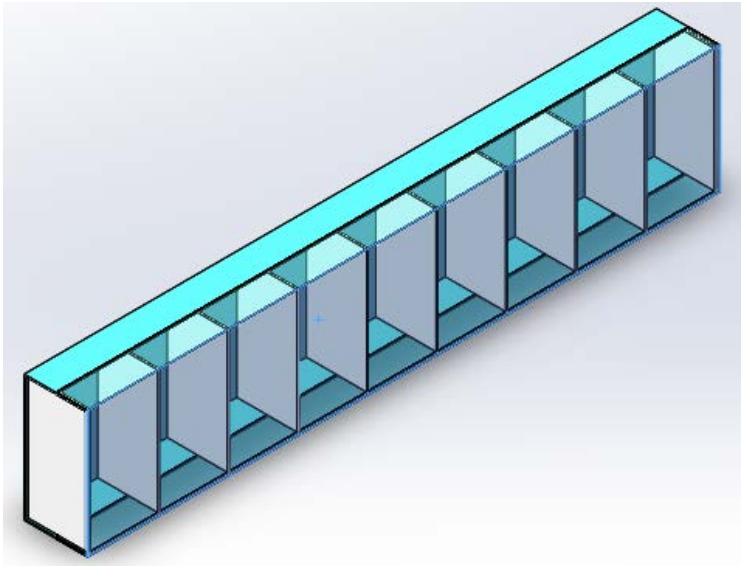

Fig 3.8 – The support plates of C-spar

Because it’s double C-spar, so applying the force is 3,500,000 N. As presented in the figure 3.9, figure 3.10, the total deformation and equivalent stress show the effects of C-spar with the supporting plates.

Figure 3.9 shows the total deformation of C-spar when the support plates are installed, minimum deformation 0 m, maximum deformation is 0.081381 m, average deformation 0.034974 m.

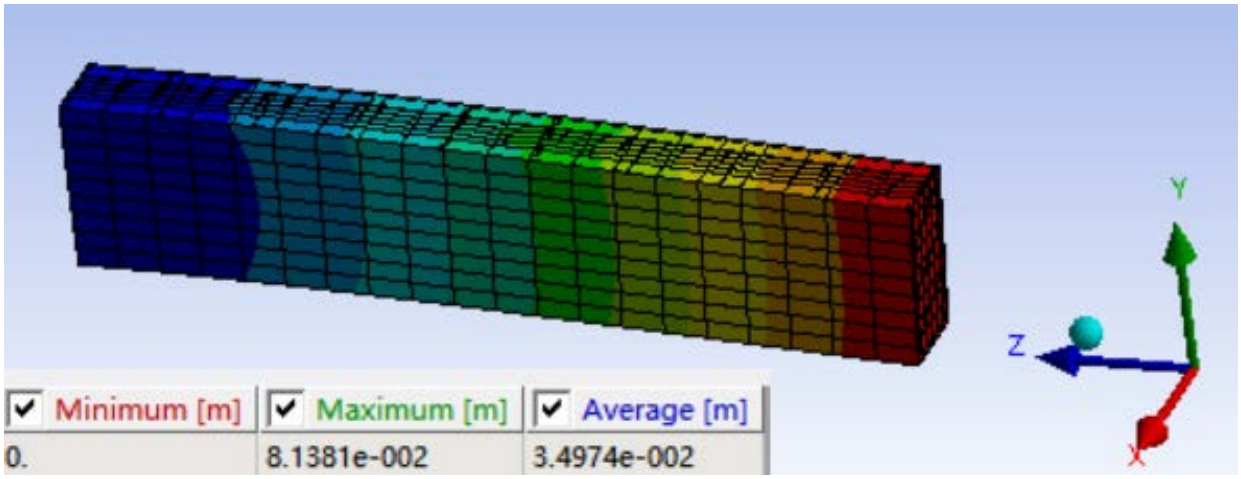

Fig 3.9 – Total deformation of C-spar when the support plates are installed

Figure 3.10 shows the equivalent stress of C-spar, minimum equivalent stress 0.20274 MPa, maximum equivalent stress is 0.23649 GPa, average equivalent stress 0.046234 GPa. Stress is mainly concentrated at the root.

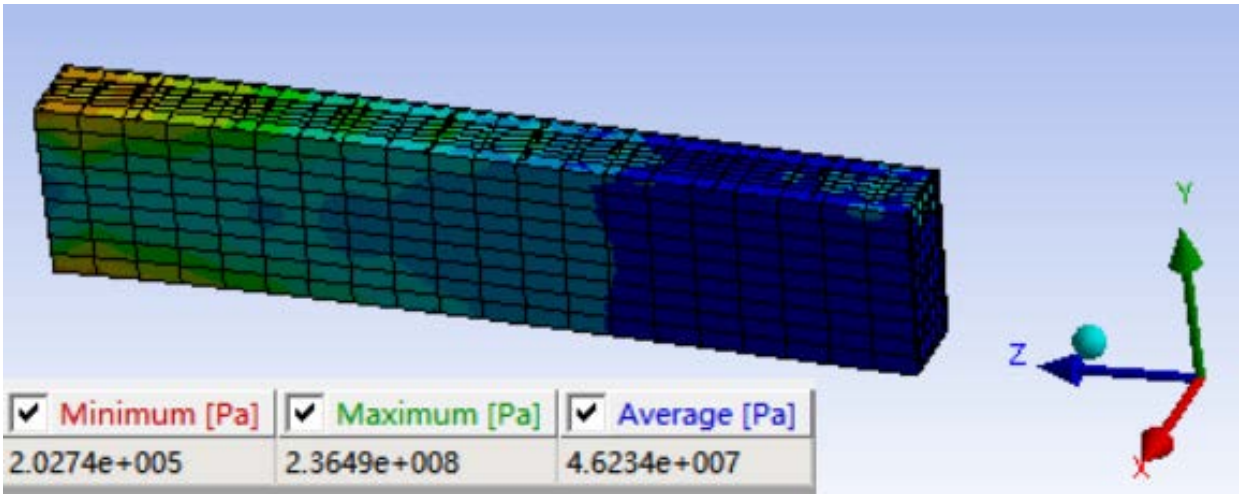

Fig 3.10 – Equivalent stress of C-spar when the support plates are installed

Because it is still single I-spar, just with some supporting plate, so applying the force is still 1,750,000 N. To use Ansys to simulate it. According to the new data from the simulations, table 3.5 can be generated.

Table 3.5

Total deformation and equivalent stress of C-spar and I-spar when the support plates are installed

Parameters / Spars	Minimum deformation (m)	Maximum deformation (m)	Average deformation (m)	Minimum Equivalent stress (MPa)	Maximum Equivalent stress (GPa)	Average Equivalent stress (GPa)
C-spar	0	0.081381	0.034974	0.20274	0.23649	0.046234
I-spar	0	0.081424	0.035031	0.16678	0.23341	0.046657

It can be seen from Tables 3.5 that the bending resistance of C-spar and I-spar are almost the same under the same support conditions. And in the simulation results, the concentrated stress of both is at the root, and there is little difference.

Under the condition that the bending resistance is almost the same, we analyze the shear stress of C-spar and I-spar.

Figure 3.11 shows the shear stress of C-spar, minimum shear stress -0.084615 GPa, maximum shear stress is 0.084615 GPa, average shear stress 0.027466 MPa.

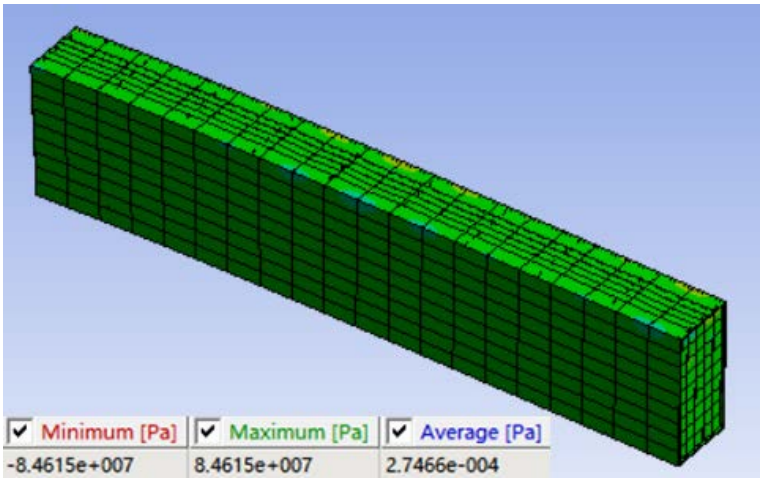

Fig 3.11 – Shear stress of C-spar

Figure 3.12 shows the shear stress of I-spar, minimum shear stress -0.084257 GPa, maximum shear stress is 0.084257 GPa, average shear stress 0.00010087 MPa.

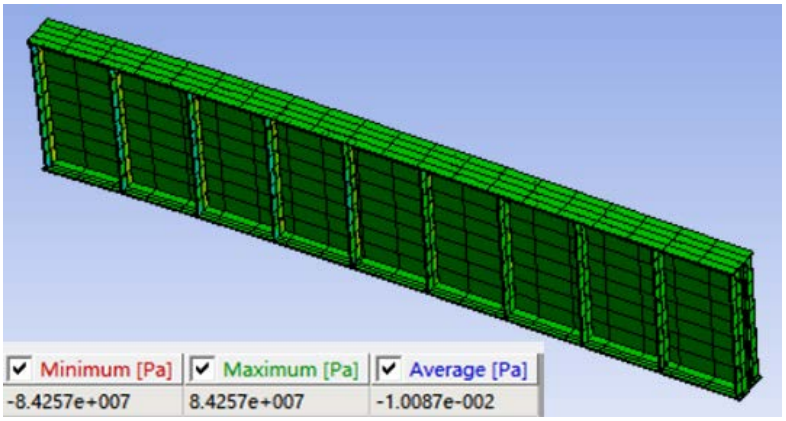

Fig 3.12 – Shear stress of C-spar

The data about shear stress of C-spar and I-spar is shown in the table 3.6.

Table 3.6

Shear stress of C-spar and I-spar

Parameters / Spars	Minimum shear stress (GPa)	Maximum shear stress (GPa)	Average shear stress (MPa)
C-spar	-0.084615	0.084615	0.027466
I-spar	-0.084257	0.084257	0.00010087

It can be seen from the table 3.6 that the shear stress of C-spar and I-spar is not much different, even though their average shear stress is quite different. However, according to Figure 3.11 and Figure 3.12, there is no excessive concentration of shear stress, so it will not cause material failure.

The spar is mainly subjected to bending moments and shear forces. However, because the wing area is too large and the wingspan is too long, which will cause the uneven force on the wing, there will also be torque generated. Therefore, when the abilities to resist bending moment and shear after adding support are similar, consider the ability of C-spar and I-spar to resist torque. In order to simplify the simulation difficulty, this section will only apply a torque of 100000N to simulate.

Figure 3.13 shows the total deformation of C-spar when a torque is applied, minimum deformation 0 m, maximum deformation is 0.16025 m, average deformation 0.039539 m.

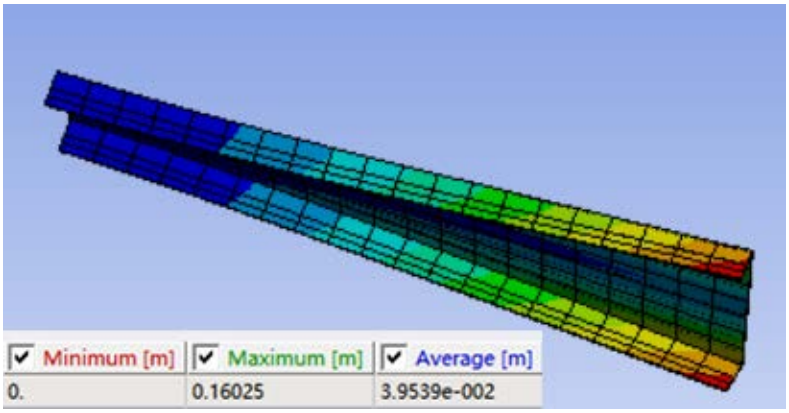

Fig 3.13 – Total deformation of C-spar when a torque is applied

Figure 3.14 shows the equivalent stress of C-spar when a torque is applied, minimum equivalent stress 0.39177 MPa, maximum equivalent stress is 0.14549 GPa, average equivalent stress 0.021617 GPa.

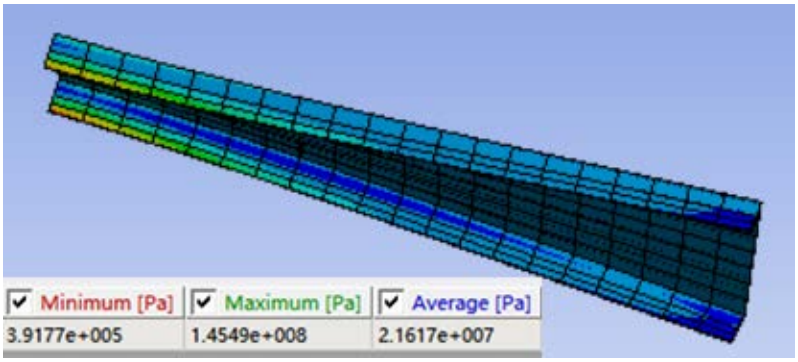

Fig 3.14 – Equivalent stress of C-spar when a torque is applied

Applying same torque to I-spar, then do simulation. The data is shown in Table 3.7.

Table 3.7

Total deformation and equivalent stress of C-spar and I-spar when a torque is applied

Parameters / Spars	Minimum deformation (m)	Maximum deformation (m)	Average deformation (m)	Minimum Equivalent stress (MPa)	Maximum Equivalent stress (GPa)	Average Equivalent stress (GPa)
C-spar	0	0.160251	0.039539	0.39177	0.14549	0.021617
I-spar	0	0.24616	0.082022	0.29567	0.18268	0.038515

From the maximum deformation and maximum equivalent stress of C-spar and I-spar in Table 3.7, it is not difficult to see that the C-beam has better anti-torque performance. Therefore, from the overall mechanical performance, C-spar is more suitable for aircraft wing spar.

3.3 Spar model with reference to A350 real spar design

In the previous chapter, it was verified by finite element simulation that the comprehensive mechanical performance of C-spar performed better than other shapes of spar. So this chapter will apply composite materials to the tapered C-spar and try to restore its performance in the real A350 wing design as much as possible. And the spars of the A350 is made of Epoxy Carbon (M21/IMA).

The force of the spar is that the flange bears the axial force caused by the bending moment; the web bears the shear stress and transmits the aerodynamic load perpendicular to the airfoil. It can be seen from the key points of the layup of beam structures in the literature [19] that the layup ratio of the flange part is generally: 60/30/10, of which 0° layup accounts for 60%, ±45° layup accounts for 30%, and 90° layup accounts for 10%; the web layup ratio is generally: 10/80/10, of which 0° layup 10% ply, 80% ±45° ply, 10% 90° ply, or all ±45° ply. In this paper, the flange part of the beam will use a layup ratio that roughly satisfies 60/30/10, and the web part will use a layup of ±45°.

This chapter uses root spar for research. In the actual design of the A350 wing, the root spar is ten meters long and tapers from the bottom to the top.

According to the equation of the wing flex (X=5*L/30), the maximum displacement of the root spar in the force direction is 1.667 m.

Other design data for the root spar can be derived from the equations in chapter 2. The cross-sectional dimensions of the root spar are shown in the figure 3.15.

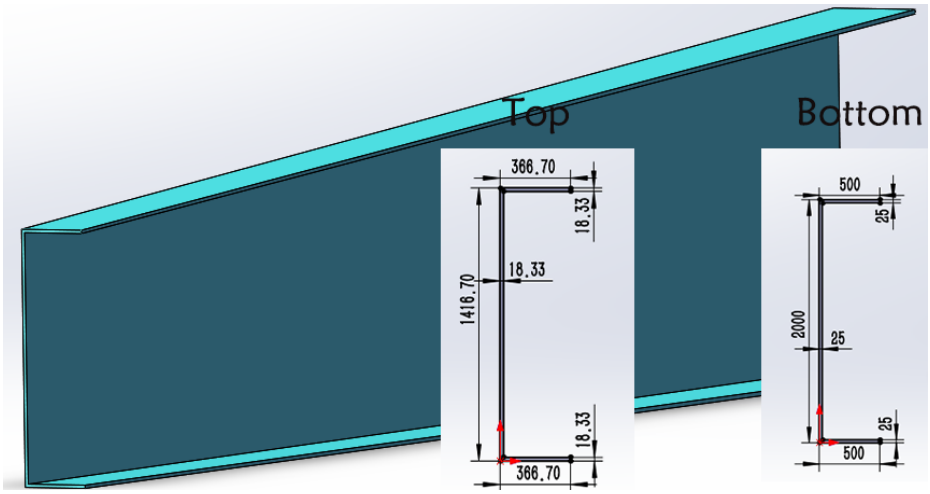

Figure 3.15 – Cross-sectional dimensions of the root spar

Then the C-spar was symmetrical and ten support plates were added to obtain an assembly, as shown in the figure 3.16.

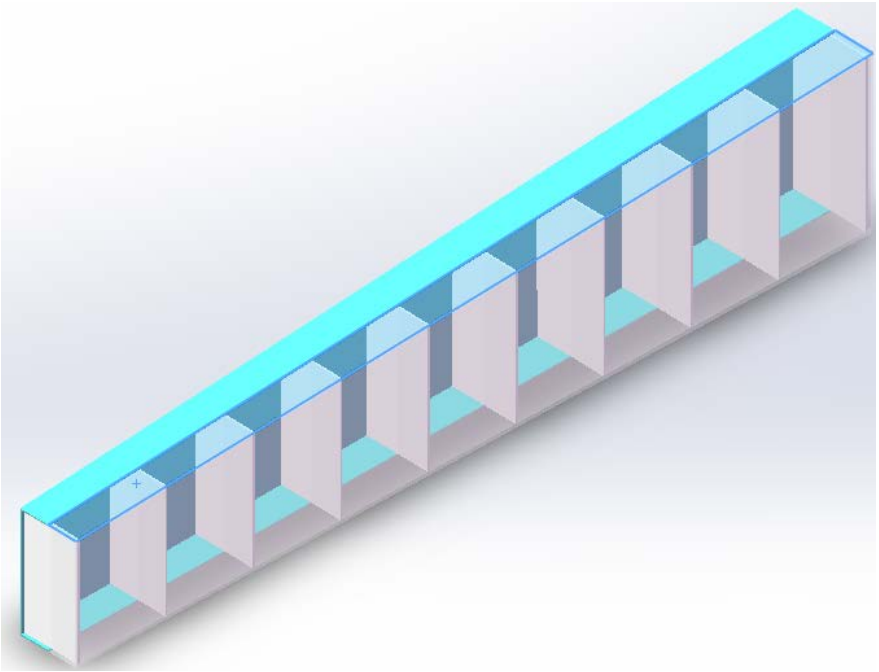

Figure 3.16 – Double tapered C-spar with supporting plates

3.4 Analysis of C-spar with different materials

Model has been created and the application of the force will be based on the equation (F=175,000-5,000*L). Ansys cannot apply force according to function, but can apply pressure according to function. So according to Pressure=Force/Area, which can get the function about pressure. But since both the area and the force are changing. It is difficult to obtain the load that varies with distance. This chapter will simplify the load. Assuming the load decreases uniformly with distance, The equation is P=350,000-1000*L. Figure 3.17 shows the variable load.

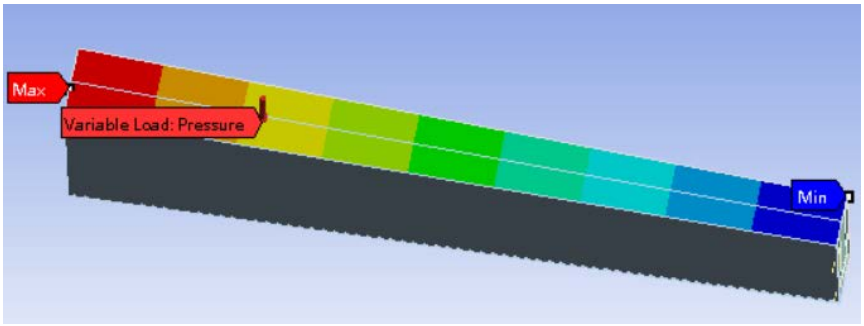

Figure 3.17 – Variable load

The mechanical properties of M21/IMA are shown in the table 3.8

Table 3.8

Mechanical properties of the M21/IMA

Density	1580 kg/m³
Young's Modulus X direction	2.09E+11 Pa
Young's Modulus Y direction	9.45E+09 Pa
Young's Modulus X direction	9.45E+09 Pa
Poisson's Ratio XY	0.27
Poisson's Ratio YZ	0.4
Poisson's Ratio XZ	0.27
Shear Modulus XY	5.5E+09 Pa
Shear Modulus YZ	3.9E+09 Pa
Shear Modulus XZ	5.5E+09 Pa

When C-spar uses the composite materials, the weight is 873.97 kg. Figure 3.18 shows the total deformation of C-spar. Minimum deformation 0 m, maximum deformation is 0.56969 m, average deformation 0.21738 m.

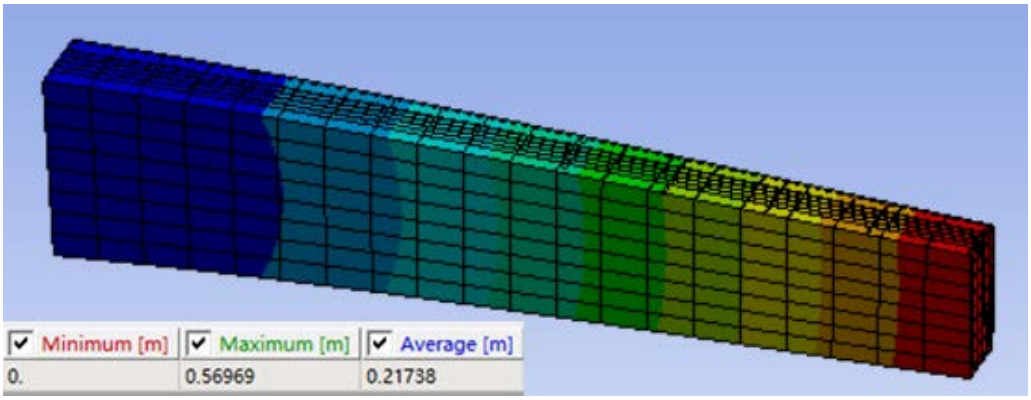

Figure 3.18 – Total deformation of tapered C-spar when using the composite materials

Figure 3.19 shows the equivalent stress of C-spar, minimum equivalent stress 0.41943 MPa, maximum equivalent stress is 0.8952 GPa, average equivalent stress 0.08341 GPa. It can be seen from the figure that the maximum equivalent stress is mainly concentrated at

the junction of the two spars. But from the color of the figure, the maximum equivalent stress does not exceed the failure criterion of the composite material.

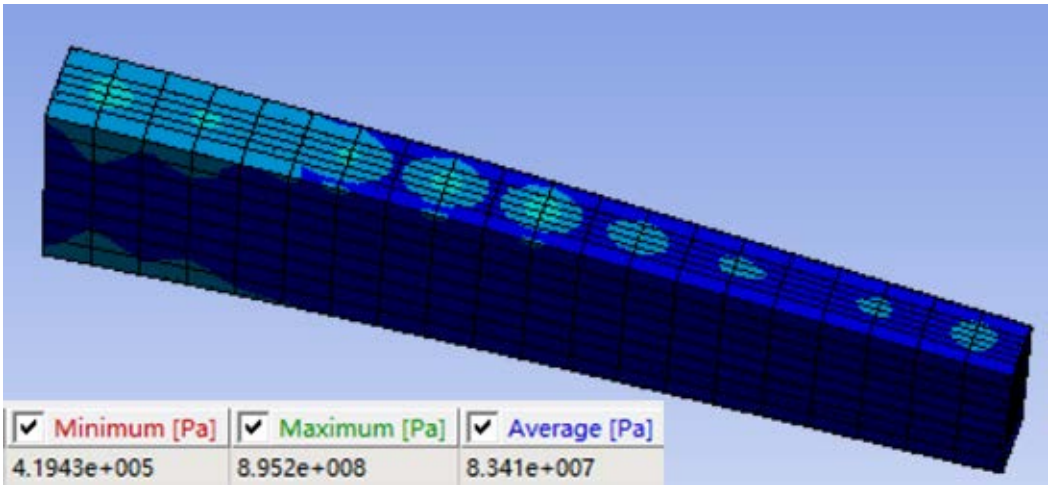

Figure 3.19 – Equivalent stress of tapered C-spar when using the composite materials

When C-spar uses the Al 7075-T6, the weight is 1554.3 kg. Figure 3.20 shows the total deformation of tapered C-spar. Minimum deformation 0 m, maximum deformation is 0.079479 m, average deformation 0.030605 m.

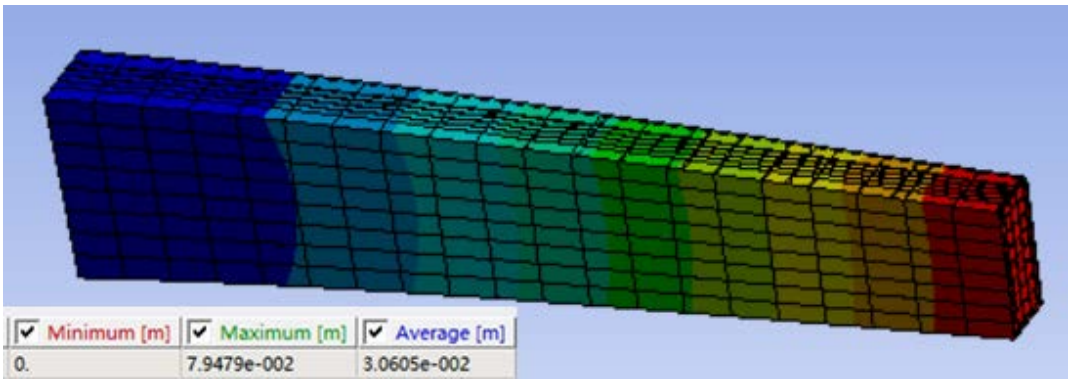

Figure 3.20 – Total deformation of tapered C-spar when using the Al 7075-T6

Figure 3.21 shows the equivalent stress of C-spar when applying Al 7075-T6, minimum equivalent stress 0.39741 MPa, maximum equivalent stress is 0.19787 GPa, average equivalent stress 0.045053 GPa. It can be seen from the figure that the maximum equivalent stress is mainly concentrated at the root of the spars. And from the color of the

figure, the red color shows the maximum equivalent stress is too concentrated, which will cause the material to yield and lead to structural failure.

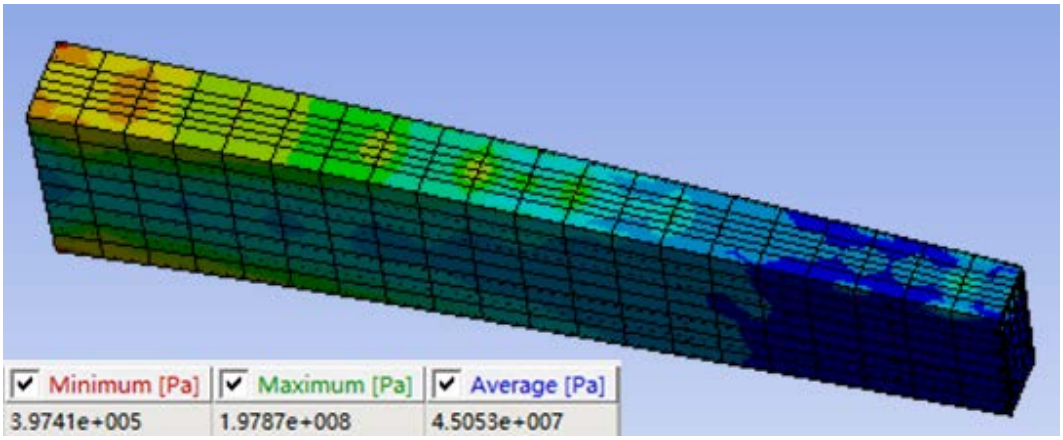

Figure 3.21 – Equivalent stress of tapered C-spar when using the Al 7075-T6

In order to more intuitively compare the C-spar with different materials, all data about weight, resistance to bending moment and stress concentration will be presented in the table 3.9.

Table 3.9

C-spar with different materials

Materials / Parameters	M21/IMA	Al 7075-T6
Density	873.97 kg	1554.3 kg
Minimum deformation (m)	0	0
Maximum deformation (m)	0.56969	0.079479
Average deformation (m)	0.21738	0.030605
Minimum Equivalent stress (MPa)	0.41943	0.39741
Maximum Equivalent stress (GPa)	0.8952	0.19787
Average Equivalent stress (GPa)	0.08341	0.045053

From Table 3.9, it can be concluded that the use of composite materials has the following advantages. Under the same volume, the weight reduction ratio is nearly 77.8%. And due to the excellent mechanical properties of composite materials, the equivalent stress

does not exceed the allowable stress of the material, and there is no obvious stress concentration phenomenon. However, from figure 3.21, we can see that when the C-spar uses the aluminum alloy, the root of C-spar has obvious stress concentration phenomenon. In the case of relatively concentrated stress, it is easy to cause material failure, which will affect the safety of the aircraft.

From the perspective of deformation, the composite material has relatively poor resistance to deformation. And according to the experimental results. Although the deformation is large, but due to the mechanical properties are excellent, so there is no stress concentration phenomenon. And the c-spar using composite materials does not exceed the maximum deformation 1.667 m of the wing design.

Because the exact design dimensions of the root spar are not known, it is still heavier than the real root spar even when composite materials are applied. However, comparing the simulation data, the purpose of verifying the advantages of composite materials has been achieved.

Fatigue strength is important whenever significant deflection occurs over the life of the component. During fly, the spar will fail when it is deflected and released multiple times, even without significant stress. This phenomenon is called "fatigue". Fatigue failure is a fracture because it undergoes numerous cycles at a stress below the yield strength of the material. Fatigue occurs because microcracks develop on the surface of the spar when subjected to cyclic stress. With repeated bending, these cracks propagate through the thickness of the spar to the point where the remaining intact structure fails by ordinary fracture (because it can no longer support the load).

But CFRPs have very different properties and designs principles. They have high fatigue resistance when free from defects and stress concentrations, but they are susceptible to impact damage, subsequent cracking and delamination. The damage growth − which need not be by fatigue −is difficult to predict. Other related problems are inspection reliability and difficulties in analyzing complex components to predict the onset of failure [29].

Conclusion to the part 3

From the results of many simulations by Ansys, under the condition of no support, I-spar and tube-spar have better comprehensive mechanical properties and can maintain their own balance. But from the perspective of wing installation and the space occupied by the spar, tube-spar is not easy to install and takes up a lot of space, So I-spar is better than tube-spar.

Box-spar is just normal, C-spar is the worst, and both have poor stability and are prone to torsion.

Therefore, under comprehensive consideration, I-shaped spar are the most suitable for the design requirements. But Boeing 787 and Airbus 350 both chose C-shaped wing spar, the C-spar must have its advantages under the condition that the torque is balanced.

After both C-spar and I-spar are added with support plates and the two sides are symmetrically arranged, the simulation results show that C-spar has almost the same mechanical properties as I-spar. But when considering the ability of their ability to resist torque, C-spar performs better than I-spar. Therefore, under comprehensive consideration, the overall mechanical properties of C-spar are the best.

Compared with aluminum alloy materials, composite materials have better mechanical properties. Even the composite material has relatively poor resistance to deformation. But due to it is mechanical properties are excellent, so there is no stress concentration phenomenon. And under the same volume, the weight reduction ratio of composite materials is nearly 77.8%.

PART 4. ENVIRONMENTAL PROTECTION

4.1 ICAO requirements towards Climate Change

We often think of human-caused climate change as something that will happen in the future, but it is an ongoing process. Today, ecosystems and communities around the world are affected.

The impact of aviation on climate change is numerous. But the most concerning is its contribution through carbon dioxide emissions. Most flights are powered by jet gasoline – although some use biofuels – which turn into carbon dioxide when burned.

As shown in figure 4.1, time series of global aviation emissions since 1940. Global aviation (both passenger and cargo) emitted an estimated 1.04 billion tons of carbon dioxide in 2018.

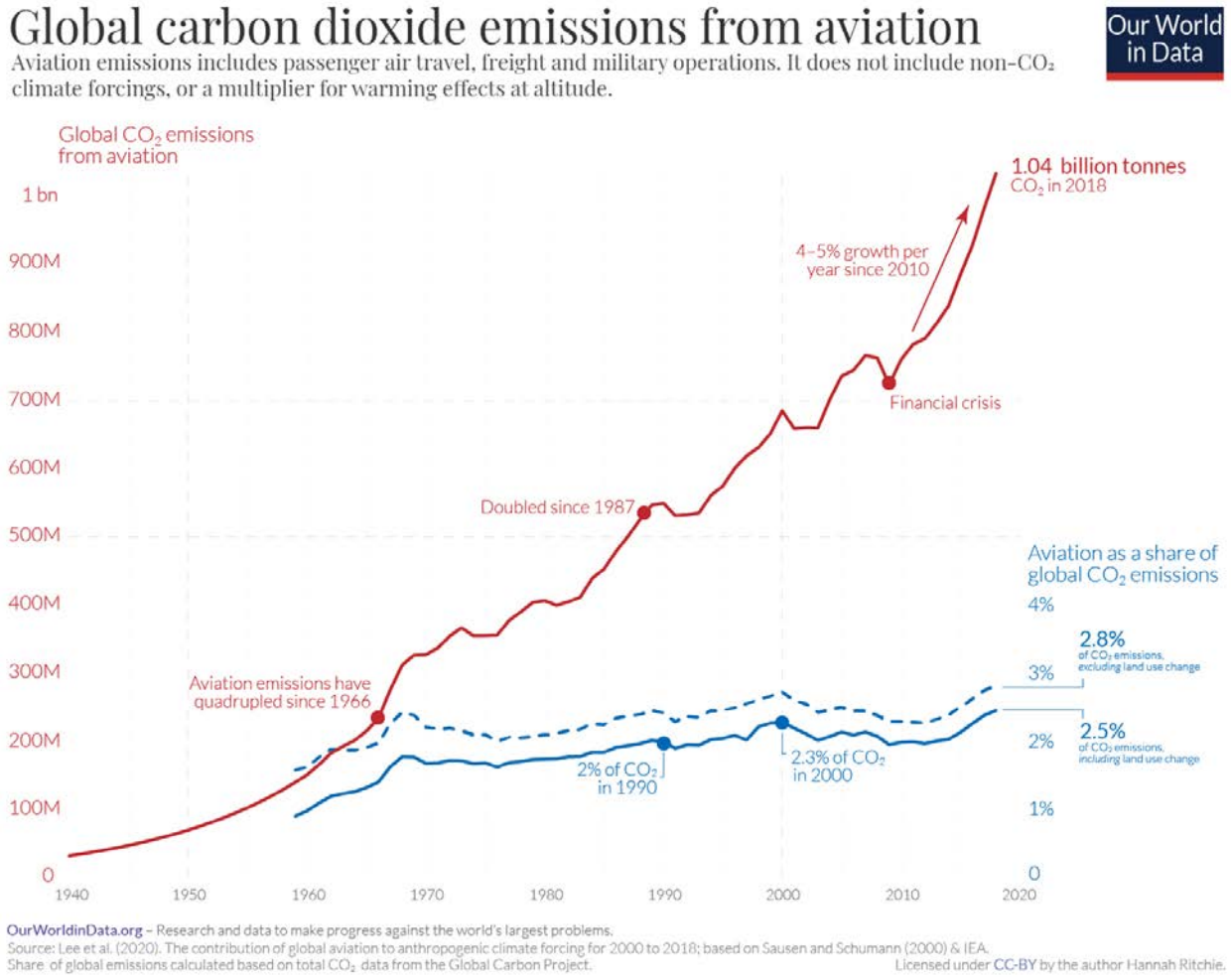

Figure 4.2 - Global carbon dioxide emissions from aviation

This accounted for 2.5% of total CO2 emissions in 2018, and aviation emissions have doubled since the mid-1980s. However, they have been growing at a similar rate to total CO2 emissions - meaning its share of global emissions has remained relatively stable: in the range of 2% to 2.5% [30].

Since the 36th ICAO Assembly in 2007, the issue of aviation emission reduction has become the focus of attention.

According to the relevant data of the International Civil Aviation Organization, the International Energy Agency and other institutions, the international air transport of most developed countries has entered a stage of slight growth in traffic volume, and fuel consumption and emissions are close to peak or even negative growth, and the future development requirements and emission reduction pressures are relatively limited; With the improvement of national income and changes in consumption structure, developing countries, especially emerging economies, have increased demand for air transport year by year, and fuel consumption and emissions have risen rapidly, facing many challenges brought about by rapid development. Since international aviation in developing and developed countries is at different stages of development. The parties have major differences in the principles, responsibility sharing and specific design of the international aviation market measures. ICAO and member states have invested a lot of energy to form a solution acceptable to all parties.

In 2007, the 36th ICAO Assembly officially launched the ICAO political negotiation process on climate change. The Assembly adopted Resolution A36-22, which recognized both the "community" principle and the "non-discrimination" principle, as well as a package of action arrangements. Economies state reservations to the clauses on the avoidance of unilateral action.

In 2010, the 37th ICAO Assembly passed Resolution A37-19, but the paragraphs on objectives, micro-exemptions and market mechanisms were reserved by nearly 60 countries. From 2011 to 2013, the EU's unilateral implementation of the emissions trading system was jointly opposed by many parties, and there was a strong voice for seeking a multilateral solution in the International Civil Aviation Organization (ICAO).

At the 38th ICAO Assembly in 2013, various parties had fierce confrontations on the core elements and design principles of the market mechanism, and the International Civil Aviation Organization (ICAO) launched a voting mechanism. Resolution A38-18, which was formed after multiple rounds of voting, proposes to establish a global international aviation market mechanism, complete the plan design in 2016, and implement it from 2020. At the same time, it proposes 16 design principles including the principle of "common zone". After the meeting, nearly 60 countries still expressed reservations on the target paragraph and the "common zone" principal paragraph of the resolution.

The climate change negotiations at the 39th ICAO Assembly achieved positive results. On October 6, local time in Montreal, Canada, the "Consolidated Statement of ICAO's Continuing Policies and Practices on Environmental Protection - Climate Change" and the "Consolidated Statement of ICAO on Environmental Protection" were adopted. These two important documents, "Consolidated Statement on Environmental Protection Continuing Policies and Practices - Global Market Measure Mechanism", have formed the world's first market mechanism for emission reduction industries.

It is reported that the market mechanism resolution adopted by the General Assembly aims to control the growth of greenhouse gas emissions from international aviation through a carbon offset mechanism. 2026) and Phase II (2027-2035). In the trial period and the first stage, countries voluntarily participate, and developed countries take the lead in participating; in the second stage, countries with a global share of more than 0.5% of international aviation activities or countries with a cumulative global share of more than 90% of international aviation activities participate. The offsetting responsibility is shared according to the average growth rate of the industry, and the proportion of responsibility shared according to the individual growth rate will be appropriately increased after 2030, which generally reflects the common but differentiated responsibilities of developed and developing countries. The resolution also stressed the need to provide assistance to countries, especially developing countries, to participate in the mechanism, and to review the implementation and impact of the mechanism every three years.

To minimize the adverse impact of international civil aviation on the global climate, ICAO develops policies, develops and updates aircraft emissions Standards and Recommended Practices (SARPs), and conducts outreach activities. These activities are carried out by the Secretariat and the Committee on Aviation and Environmental Protection (CAEP). In carrying out its activities, ICAO also cooperates with other UN agencies and international organizations.

The ICAO Assembly, at its 40th Session in 2019, adopted Resolution A40-18: Consolidated Statement of Continuing ICAO Policies and Practices Related to Environmental Protection – Climate Change. It reaffirms the two global aspirational goals set by the international aviation industry at the 37th General Assembly in 2010, namely a 2% annual increase in fuel efficiency by 2050 and carbon neutral growth from 2020 onwards.

4.2. Ways to Climate Change

As presented in figure 4.2, to achieve global aspirational goals and promote sustainable growth in international aviation, ICAO is pursuing a package of measures including technical improvements in aircraft, operational improvements, market-based measures (CORSIA) and sustainable aviation fuels [31].

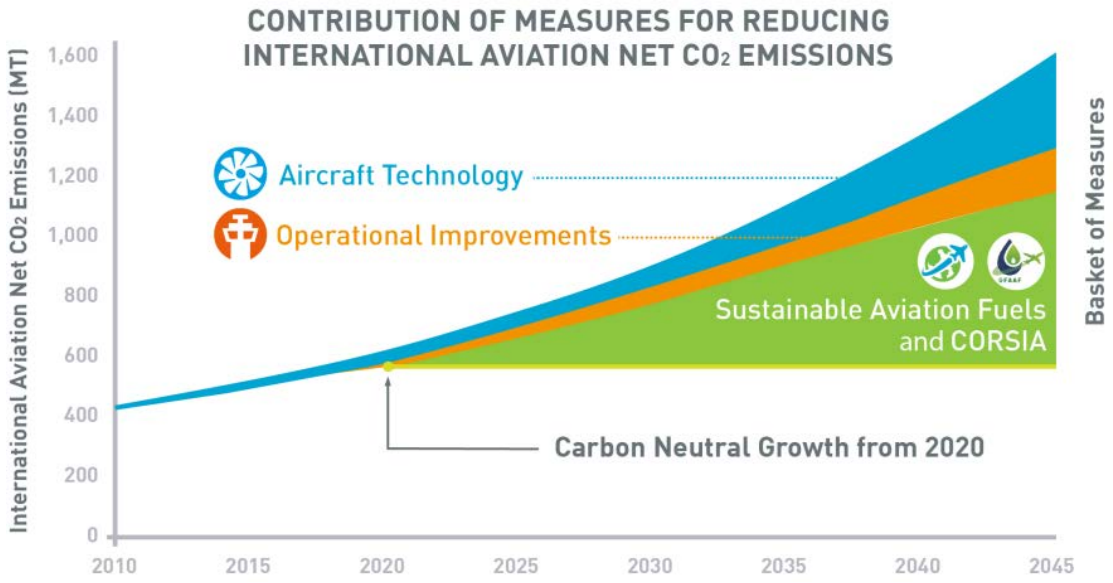

Figure 4.2 - Measures for reducing International Aviation NET CO_2 Emission

1. Technical improvements: Through the Sustainable Flight National Partnership, NASA and the FAA are working with industry to accelerate the development of more efficient aircraft and engine technologies, with the goal of saving up to 30% in fuel compared to today's aircraft, it also provides significant noise reduction and emission reduction benefits. New, more efficient narrow-body aircraft could enter the U.S. fleet in the 2030s, while new wide-body aircraft could enter the U.S. fleet in the 2040s.

Airbus has also already contributed to progress in reducing noise and emissions from new aircraft. For example, the A350 XWB reduces fuel burn and CO2 emissions by 25 percent compared to previous generations of aircraft. Likewise, the A330neo reduces average fuel consumption per seat by 25 percent compared to previous models in its class.

Electric and hybrid: Airbus has been developing these systems since 2010 and in November 2017 launched a hybrid prototype, the E-Fan X, in partnership with Rolls-Royce. The maiden flight is expected in 2021. Airbus has also developed two VTOL prototypes, Vahana, an all-electric single-seat tilt-wing aircraft that has flown more than 80 times so far; and City Airbus, an all-electric four-seater helicopter, which made its first flight in May 2019. Maybe they are the self-driving taxis of the future. In 2018, the company's solar-powered high-altitude pseudo-satellite drone Zephyr set a record for the longest flight time of an aircraft.

New energy-saving and environmentally friendly materials: Airbus is considering a variety of materials, including lightweight and functional composite materials. Such as carbon fiber reinforced plastic (CFRP), this material has better fatigue and corrosion resistance, so it can last longer than traditional metal materials, and can save weight and fuel significantly. Companies are also looking for bioderived materials, such as spider silk (which is stronger than steel, tougher than Kevlar fiber, and extremely lightweight), which promises to revolutionize aerospace design. The company is also experimenting with advanced surfaces and coatings with ultra-high temperature materials and ceramics. These new surfaces and materials, such as tungsten carbide coatings and new metal alloys, can be used in critical aircraft

components such as compression flap pads and turbine blades to provide greater efficiency and replace environmentally damaging materials.

2. Operational improvements: Improved operational efficiency, while the US National Airspace System is efficient, there are opportunities to reduce fuel burn during all phases of flight. These include improving efficiency during taxi, takeoff and landing, as well as optimizing flight trajectories. Research has shown that aircraft operations also affect climate through non-CO2 emissions, particularly through contrails and aviation-induced clouds — thread-like clouds that form behind jet engines when hot exhaust gas mixes with cooler surrounding air. The U.S. government is supporting research to cost-effectively reduce some of aviation's climate impact by limiting the formation of contrails.

When parked at the airport gate, the aircraft must be powered to provide air conditioning and electricity and start the engines. At the tail of the aircraft is a small generator called an auxiliary power unit (APU). Many airports are now equipping gates with fixed ground power and pre-conditioned air, allowing pilots to turn off the APU on the ground, saving fuel and noise. Airports are also working to make ground service equipment (baggage loading equipment, catering trucks, passenger cars) more energy efficient using natural gas or electricity.

Departure. There are technologies in operation as aircraft taxiing from the gate to the runway, such as single-engine taxiing, or in development, such as autopilot devices that allow aircraft to reach the runway without using full engine power. Airports, airlines and air navigation service providers are also collaborating on so-called "green takeoffs," where planes can take off and climb at a steady pace to get to the most efficient phase of flight, cruise, more quickly.

Cruise. Planes still burn less fuel with less weight onboard, so airlines are looking for ways to reduce the weight of carrying a lot of items — from food service trolleys to seats and carpets to just the right amount of weight load the amount of water per flight instead of filling the tank every time. This results in significant savings. Airlines and air traffic controllers are also working together to take advantage of weather conditions at high altitudes. Pilots and flight planners have been studying wind

patterns before takeoff and guiding the plane along strong wind currents. The use of airflow reduces flight time and emissions, although at times longer distances are flown. Flexible routing is also happening now, especially on long-distance routes in uncrowded airspace, but new surveillance technology similar to GPS systems will enable it to be used on more congested routes.

Arrival. Traditionally, flights have taken several steps to descend from cruise to landing, descending from one altitude to the next, and then "levelling" by starting the engines. New technology can more accurately monitor the position of each aircraft, providing a more comprehensive picture of the traffic environment. This has led to a new technology - continuous descent operation - that allows the aircraft to almost "taxi" into the airfield with the engines set very low. Not only does this save fuel, it also reduces the impact of noise on the surrounding community. It is now used more and more all over the world depending on weather and traffic conditions.

3. Market-based measures (CORSIA): The government provides incentives to reduce airport emissions through a number of programs, including the emission trading scheme (Cap and Trade) and Green-tax.

Emissions trading schemes (ETS), also known as cap-and-trade, involve setting an overall limit on emissions and then allowing companies to buy and sell emissions allowances to meet their own goals. A global ETS is one possible option for ICAO to reduce emissions.

ETS provides companies with an economic incentive to fight global warming, because emissions allowances have cash value, so companies that reduce their own emissions can sell unused credits to companies that exceed their emissions.

The green tax increases the cost of each flight by adding a fee for each passenger, each departure or landing, or each flight segment. The green tax is designed to reduce demand for air travel, which simply means pricing some passengers out of the market. But in many cases, passengers have no reasonable alternative to air transportation.

4. Sustainable aviation fuels: Sustainable fuels as shown in figure 4.3 [32] Sustainable fuels produced from renewable and waste feedstocks can provide the greatest impact on our efforts to reduce aviation greenhouse gas emissions.

Pathways and processes	Feedstock options	Producers using the pathway	Date of approval	Current blending limit
Fischer-Tropsch Synthetic Paraffinic Kerosene (FT-SPK)	biomass (forestry residues, grasses, municipal solid waste)		2009	up to 50%
Hydroprocessed Esters and Fatty Acids (HEFA-SPK)	algae, jatropha, camelina	Alt Air	2011	up to 50%
Hydroprocessed Fermented Sugars to Synthetic Isoparaffins (HFS-SIP)	microbial conversion of sugars to hydrocarbon	Amyris	2014	up to 10%
FT-SPK with aromatics (FT-SPK/A)	renewable biomass such as municipal solid waste, agricultural wastes and forestry residues, wood and energy crops		2015	up to 50%
Alcohol-to-Jet Synthetic Paraffinic Kerosene (ATJ-SPK) [isobutanol]	agricultural waste products (stover, grasses, forestry slash, crop straws)	Gevo	2016	up to 30%
Alcohol-to-Jet Synthetic Paraffinic Kerosene (ATJ-SPK) [ethanol]	agricultural waste products (stover, grasses, forestry slash, crop straws)	LanzaTech	2018	up to 50%
Catalytic hydrothermolysis synthetic jet fuel (CHJ)	Triglyceride-based feedstocks (plant oils, waste oils, algal oils, soybean oil, jatropha oil, camelina oil, carinata oil and tung oil)	ARA and Euglena	2020	up to 50%
High Hydrogen Content Synthetic Paraffinic Kerosene (HHC-SPK)	biologically derived hydrocarbons such as algae	IHI World	2020	up to 10%

Figure 4.3 - Sustainable fuels

These fuels are critical to the aviation industry's ability to meet net-zero emissions targets, and they have the potential to reduce emissions by up to 100% on a life cycle basis. Sustainable aviation fuel can be used in today's aircraft fleet without modification and can be produced from a variety of feedstocks, including waste, residue, biomass, sugar, oil and gaseous carbon sources.

Conclusion to the part 4

The aviation industry has made significant strides in fuel and CO2 efficiency, using half the amount of fuel per flight compared to 1990. In other words, our flight today produces only 50% less carbon dioxide than the same flight in 1990. This has been achieved through technological advancements and improvements in operations and infrastructure.

Trade and tourism are important drivers of global economic development, and as more people get richer, so does their desire to travel the world. The industry's Climate Action Framework is designed to help find a balance between two goals - enabling economic growth through connectivity and reducing climate impact.

PART 5. LABOUR PROTECTION

5.1. Introduction

For workers, the workplace is an essential part of the work period. This workplace can be thought of as a typical open office area. For an engineer, the workplace includes a typical office chair, desk and computer. Design engineers working in front of personal computers are their main work. Therefore, the working conditions of a typical office space layout will be discussed and analyzed.

5.2. Working place

Design engineer workplaces are mostly located in the open office area. About the open office area, the size of the passage in the office should not be less than 0.9m, so that two people can pass through the front and side at the same time. The working aisle between two desks should not be less than 1.2m. The distance between the passage with the filing cabinet and the desk should not be less than 1.0m to ensure the normal movement of employees after the cabinet door is opened. The standing distance of the work post is 0.75m, which is convenient for people to move around.

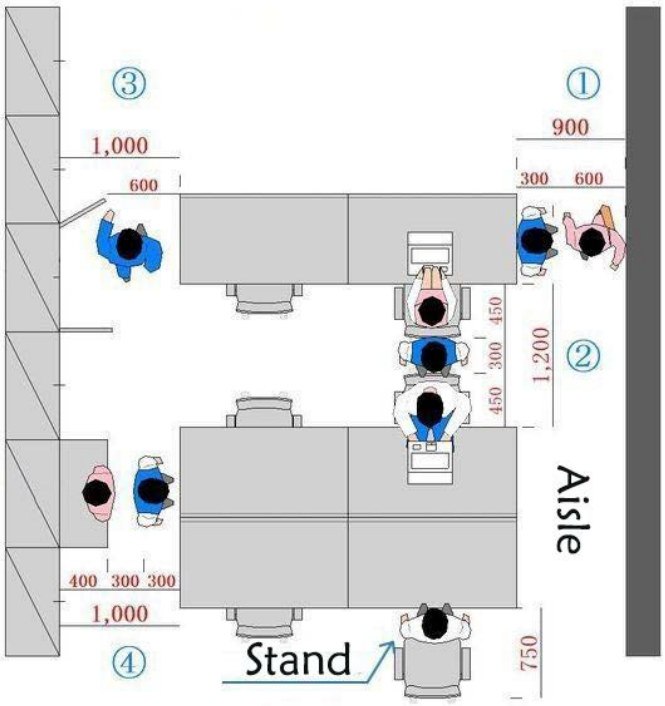

Figure 5.1 - Open office area

The room temperature is usually 24-26 ℃ in the warm period, 19-23 ℃ in the cold period, and the indoor relative humidity is usually 40-60%. The main source of indoor noise pollution is the noise of computers and printers. Also, if available, there is a carbon fire extinguisher in the corner of the room to put out the fire.

5.3. Harmful and hazardous working factors

In the process of production and labor, there are factors that have a harmful effect on the health and labor ability of employees and cause diseases. In order to distinguish the characteristics and effects of the adverse effects of objects on the human body, they are divided into risk factors (emphasis on sudden and instantaneous effects) and harmful factors (emphasis on cumulative effects within a certain time range). Sometimes the two are not distinguished and are collectively referred to as risk factors. Equipment, facilities and places with objectively existing hazards, harmful substances and energy exceeding the critical value may become risk factors.

Physical harmful and hazardous factors:

1) Electrical hazards (exposed live parts, leakage, lightning, static electricity, sparks, other electrical hazards);

2) Noise hazards (mechanical noise, electromagnetic noise, hydrodynamic noise, other noise);

3) Electromagnetic radiation (ionizing radiation: ultraviolet, laser, radio frequency radiation, ultra-high voltage electric field, etc.);

4) fire;

5) Other physical harmful and hazards factors.

Chemical harmful and hazardous factors:

1) Flammable and explosive substances (flammable and explosive gases, flammable and explosive liquids, flammable and explosive solids, flammable and explosive dusts and aerosols, and other flammable and explosive substances);

2) Spontaneous flammable substances;

3) Toxic substances (toxic gases, toxic liquids, toxic solids, toxic dusts and aerosols, and other toxic substances);

4) Corrosive substances (corrosive gases, corrosive liquids, corrosive solids, other corrosive substances;

5) Other chemical harmful and hazards factors.

Biological harmful and hazardous factors:

1) Pathogenic microorganisms (bacteria, viruses, other pathogenic microorganisms);

2) Infectious disease vectors;

3) Harmful animals;

4) Harmful plants;

5) Other biological harmful and hazards factors.

Psychological harmful and hazardous factors:

1) Overload (physical overload, hearing overload, visual overload, and other overloads);

2) Psychological abnormalities (emotional abnormalities, risk-taking, excessive stress, other psychological abnormalities);

3) Identification function defects (perception delay, identification error, other identification function defects);

4) Other psychological harmful and hazards factors.

Behavioral harmful and hazardous factors;

1) Command errors (command errors, illegal command, other command errors);

2) Operation errors (mis-operations, illegal operations, other operational errors);

3) Mistakes in guardianship;

4) Other behavioral harmful and hazards factors.

Other harmful and hazardous factors.

5.4. Analysis of working conditions and development of protective measures

Take collective or individual protection measures to prevent and reduce the impact of harmful and dangerous factors of production on workers.

- Dust from certain substances, which may cause respiratory problems, nervous system problems, and loss of consciousness. To avoid this effect, it is necessary to normalize the airflow in the work area with the help of ventilation and air conditioning;

- Inadequate lighting in the work area can lead to visual comprehension problems and injuries. To avoid such problems, it is necessary to normalize the lighting levels in the workplace by adding light sources, filters, lighting protection equipment;

- Electric shock that may cause injury or death. In order to avoid the impact of electric shock on personnel, the following protective equipment can be used: the circuit is automatically closed, grounded, partially closed;

- Elevated temperature of work equipment may cause body burns or overheating. To eliminate this, workplaces must be equipped with equipment for ventilation, thermal insulation, and air conditioning.

5.5. Fire safety rules at the open office area

1. Because office electrical appliances are mostly powered by plug-ins, do not use too many electrical appliances when using them, so as to avoid overloading the plug-board and overheating and causing fire.

2. Can't just use some of the most convenient wall sockets and leave other wall sockets idle, which will cause accelerated aging of the socket's wires, and even cause accidents due to current overload.

3. Small-sized electrical appliances commonly used in office such as shredders and sealing machines have poor heat dissipation and should be disconnected from the power supply in time when not in use.

4. It is necessary to leave the seat for a long time. When the computer is not in use, set the automatic "sleep" to reduce the power consumption of the computer and avoid fire hazards; business personnel should turn off the computer when they go out, and do not let the computer stand by for a long time.

5. If there is a double-connected main switch in the office, cut off the indoor power supply when you get off work. (This is not suitable for offices with fish tanks and refrigerators)

6. When turning off the computer, you must turn off the power of the monitor and turn off each independent switch of the board at the same time.

7. After get off work, unplug the water dispenser, electric fan, air conditioner and other power plugs or turn off the power switch, which is both safe and power-saving.

8. Mobile phones, cameras and other batteries should not be charged for too long (preferably not more than six hours), and the charging battery should be unplugged when leaving get off work to prevent the battery from exploding.

9. Paper and articles should not be burned in the office.

10. Smoking is not allowed in the office. If you need to smoke, you can go to the smoking area of the floor passage. After smoking, please be sure to completely extinguish the cigarette butts to prevent fire hazards.

Conclusion to the part 5

In the chapter 5 on labor protection, the working conditions of design engineers are analyzed. From the above discussion, it can be seen that there are many unfavorable factors that affect the work of design engineers.

However, when working conditions meet regulatory requirements and the workplace is properly organized, harmful factors are eliminated or significantly reduced.

According to the literature and normative documents studied, comfortable, healthy and safe working conditions in the workplace of design engineers should be ensured.

GENERAL CONCLUSIONS

The master degree thesis consists of the following main parts: the first part concentrates on the application and development of composite materials, which introduces the developments of composite. The composite material has very excellent mechanical properties. Ideal for use in the primary structure of an aircraft and for weight reduction purposes.

The second part of master thesis is devoted to composite structures theoretical background, which introduces the basic theory of composite, stiffness analysis of laminates, thin-walled structures theories, several commonly used composite structural strength criteria and the model selection.

In the third part of the thesis, Solidworks is used to model the structural elements of the wing and Ansys is used to simulate the stress-strain state of the element under the loads. From the results of many simulations by Ansys, under the condition of no support, I-spar and tube-spar have better comprehensive mechanical properties and can maintain their own balance. But from the perspective of wing installation and the space occupied by the spar, tube-spar is not easy to install and takes up a lot of space, So I-spar is better than tube-spar. Box-spar is just normal, C-spar is the worst, and both have poor stability and are prone to torsion. Therefore, under comprehensive consideration, I-shaped spar are the most suitable for the design requirements. But Boeing 787 and Airbus 350 both chose C-shaped wing spar, the C-spar must have its advantages under the condition that the torque is balanced. After both C-spar and I-spar are added with support plates and the two sides are symmetrically arranged, the simulation results show that C-spar has almost the same mechanical properties as I-spar. But when considering the ability of their ability to resist torque, C-spar performs better than I-spar. Therefore, under comprehensive consideration, the overall mechanical properties of C-spar are the best. Compared with aluminum alloy materials, composite materials have better mechanical properties. Even the composite material has relatively poor resistance to deformation. But due to it is mechanical properties are excellent, so there

is no stress concentration phenomenon. And under the same volume, the weight reduction ratio of composite materials is nearly 77.8%.

The fourth part was devoted to the environmental protection. In this part which discusses the impact of aviation on climate change and related solutions.

The fifth part was devoted to the labor protection where it discusses the working conditions of design engineers. According to the literature and normative documents studied, comfortable, healthy and safe working conditions in the workplace of design engineers should be ensured.

REFERENCES

1. Marcelo André Santiago Barros, Roberto Tetsuo Fujiyama, Jandecy Cabral Leite. Advantages of applying composite material to replace metal alloys in aviation. January 2015, p.21–28.
2. Tim Palucka and Bernadette Bensaude-Vincent. Composites Overview. October 2002.
3. Negin Amanat Maddock, Natalie L.James, David R.McKenzie, James F.Patrick. The Design and Manufacture of Medical Devices Woodhead Publishing Reviews: Mechanical Engineering Series. 2012, p. 239–272.
4. Chantal Fualdes, Xavier Jolivet, Cedric Chamfroy. Safe operations with composite aircraft. July 2014.
5. GUIDE TO COMPOSITES. p13.
6. Sangwook Sihn, Ran Y. Kim, Kazumasa Kawabe, et al. Experimental studies of thin-ply laminated composites[J]. Compos Sci Technol. 2007, p. 996–1008.
7. Hassan M. El-Dessouky. Spread Tow Technology for Ultra Lightweight CFRP Composites: Potential and Possibilities. January 2017, p. 3–8.
8. Jen Chung Chen, Chuen Guang Chao. Numerical simulation and experimental investigation for design of a carbon fiber tow pneumatic spreading system[J]. 2005, p. 2514–2529.
9. S Sihn, R Kim, K Kawabe, S. Tsai. Experimental studies of thin-ply laminated composites, Compos. Sci. Technol. 2007, p.996–1008.
10. T Yokozeki, Y Aoki, T. Ogasawara. Experimental characterization of strength and damage resistance properties of thin-ply carbon fiber/toughened epoxy laminates, Compos. Struct. 2008, p.382–389.
11. G Guillamet, A Turon, J Costa, J Renart, P Linde, JA. Mayugo. Damage occurrence at edges of non-crimp-fabric thin-ply laminates under off-axis uniaxial loading, Compos. Sci. Technol. 2014, p. 44–50.

12. G Guillamet, A Turon, J Costa, P. Linde. A quick procedure to predict free-edge delamination in thin-ply laminates under tension, Eng. Fract. Mech. 2016, p. 28–39.
13. E Kalfon-Cohen, R Kopp, C Furtado, X Ni, A Arteiro, G Borstnar, et al. Synergetic effects of thin plies and aligned carbon nanotube interlaminar reinforcement in composite laminates, Compos. Sci. Technol. 2018, p. 160–168.
14. Yanan Yuana, Xinyue Li, Qiang Zhang, Pan Liu, Zuoqi Zhang. Dependence of damage modes on the ply-thickness of ultra-thin-ply composites. 2021, p. 3–4.
15. Benedikt Kötter, Janina Endres, Johann Körbelin, Florian Bittner, Hans-Josef Endres, Bodo Fiedler. Fatigue and fatigue after impact behaviour of Thin- and Thick-Ply composites observed by computed tomography. 2021, p. 4–5.
16. RYOKO MORISHIMA. ANALYSIS OF COMPOSITE WING STRUCTURES WITH A MORPHING LEADING EDGE. January 2011, p.74-78, 82-87.
17. Yang Naibin, Zhang Yining. Composite aircraft structure design [M] Beijing: Aviation Industry Press. 2002, p. 43-55,102, 216-219.
18. Elastic buckling of long, flat, symmetrically-laminated (AsBoDf), composite stiffened panels and struts in compression. ESDU International. 2003.
19. Wang Yaoxian. Mechanics and Structural Design of Composite Materials[M]. Shanghai: East China University of Science and Technology Press. 2012, p. 25-44,53,84-108.
20. Shen Guanlin, Hu Gengkai. Mechanics of Composite Materials[M]. Beijing: Tsinghua University Press. 2006, p. 47-57,86-103.
21. https://modernairliners.com/airbus-a350-xwb-introduction/airbus-a350-xwb-specifications/
22. https://theflyingengineer.com/2014/01/14/understanding-the-ultimate-load-wing-test-a350/
23. https://www.aerospace-technology.com/projects/a350wxb/
24. GKN A350 spar program update. January 2011.
25. A350 & A400M wing spars: A study in contrasts. January 2013.
26. Aircraft wing worker for the world. April 2010.

27. https://en.wikipedia.org/wiki/Airbus_A350#Wing
28. A350 & A400M wing spars: A study in contrasts. January 2013.
29. Russell James Hugh Wanhill. Fatigue Requirements for Aircraft Structures. November 2017, p.7-8.
30. Hannah Ritchie. Climate change and flying: what share of global CO2 emissions come from aviation? October 2020.
31. https://www.icao.int/environmental-protection/Pages/climate-change.aspx
32. https://aviationbenefits.org/environmental-efficiency/climate-action/